



Cell membrane-biomimetic coating via click-mediated liposome fusion for mitigating the foreign-body reaction



Lingbing Yang^a, Xubo Lin^a, Jin Zhou^a, Sen Hou^a, Yunnan Fang^a, Xuewei Bi^a, Li Yang^{a,c}, Linhao Li^{a,*}, Yubo Fan^{a,b,**}

^a Beijing Advanced Innovation Center for Biomedical Engineering, Key Laboratory for Biomechanics and Mechanobiology of Chinese Education Ministry, School of Biological Science and Medical Engineering, Beihang University, Beijing, 100083, China

^b School of Engineering Medicine, Beihang University, Beijing, 100083, China

^c Key Laboratory for Biorheological Science and Technology of Chinese Education Ministry, Bioengineering College, Chongqing University, Chongqing, 400030, China

ARTICLE INFO

Keywords:
Electrospinning
Liposome
Silk
Click chemistry
Foreign-body reaction
Vascularization
Macrophage polarization

ABSTRACT

The foreign-body reaction (FBR) caused by the implantation of synthetic polymer scaffolds seriously affects tissue-biomaterial integration and tissue repair. To address this issue, we developed a cell membrane-biomimetic coating formed by “click”-mediated liposome immobilization and fusion on the surface of electrospun fibers to mitigate the FBR. Utilization of electrospun polystyrene microfibrous scaffold as a model matrix, we deposited azide-incorporated silk fibroin on the surface of the fibers by the layer-by-layer assembly, finally, covalently modified with clickable liposomes via copper-free SPAAC click reaction. Compared with physical adsorption, liposomes click covalently binding can quickly fuse to form lipid film and maintain fluidity, which also improved liposome stability *in vitro* and *in vivo*. Molecular dynamics simulation proved that “click” improves the binding rate and strength of liposome to silk substrate. Importantly, histological observation and *in vivo* fluorescent probes imaging showed that liposome-functionalized electrospun fibers had negligible characteristics of the FBR and were accompanied by many infiltrated host cells and new blood vessels. We believe that the promotion of macrophage polarization toward a pro-regenerative phenotype plays an important role in vascularization. This bioinspired strategy paves the way for utilizing cell membrane biomimetic coating to resist the FBR and promote tissue-scaffold integration.

1. Introduction

Biomaterials have become more important in solving many clinical and healthcare problems, and are widely used in the fields of biomedicine. An important consideration in the design of biomaterials is the interaction between the implant materials and the host immune system [1,2]. Electrospun micro/nanofibrous scaffolds, as functional carriers for cells and drugs, have been used in a wide range of biomedical applications, including wound healing, tissue engineering, and drug delivery [3–5]. However, because the high surface area of electrospun fibers increases non-specific protein adsorption, the resulting foreign-body reaction (FBR) limits the functionality *in vivo* [6,7]. The formation of FBR mainly includes the following four steps: i. After implantation of electrospun micro/nanofibrous scaffolds, non-specific

proteins adsorb on the surface of fiber, and then the provisional matrix forms at the material-tissue interface; ii. As acute inflammation occurs, cytokines and chemokines that provisional matrix released promote the recruitment, migration, proliferation, and activation of inflammatory cells such as macrophages and neutrophils; iii. In the process of the later stage of FBR, macrophages fuse into foreign-body giant cells (FBGCs); iv. Finally, fibroblasts and myofibroblasts deposit on the surface of scaffolds, which form collagen fibrotic capsules around materials. The overall FBR process is completed within 2–3 weeks after implantation [8–10]. The formed fibrotic capsules isolate biomaterials and surrounding tissues, resulting in the significant reduction of biomaterial-tissue crosstalk and integration.

At present, researchers have found various physical, chemical, and biological methods to mitigate FBR caused by biomaterials

* Corresponding author.

** Corresponding author. Beijing Advanced Innovation Center for Biomedical Engineering, Key Laboratory for Biomechanics and Mechanobiology of Chinese Education Ministry, School of Biological Science and Medical Engineering, Beihang University, Beijing, 100083, China.

E-mail addresses: linhaoli@buaa.edu.cn (L. Li), yubofan@buaa.edu.cn (Y. Fan).

implantation. Physical methods mainly regulate physical parameters of biomaterials, which can affect macrophages polarization and reduce the formation of collagen fibrotic capsules, including the pore sizes of porous scaffolds [11,12], the stiffness of substrate materials [13,14], the sizes of particles [15], and the surface topology [16–18]; The chemical methods are mainly addition or modification of functional chemical groups [19,20], antifouling zwitterionic polymers [21,22], and natural macromolecules [23–25] to reduce the protein adsorption and cell adhesion; Biological methods are mainly regulation of macrophages polarization by immunomodulatory factors such as interleukin-4 (IL-4) and IL-10 [26–28]. Although most of the physical and chemical strategies can effectively reduce the non-specific protein adsorption and host immune cell adhesion, they may ignore the inherent host immune system response and reduce the integration of tissue-material and wound healing effect. Immunomodulators of cytokines and chemokines also have some disadvantages, such as side effects, high cost and short half-life *in vivo*. Recently, using biomimetic technology to construct *in vivo* “camouflaged” or “invisible” cell membrane-mimetic coatings is an emerging concept for the development of nanoparticles-based drug delivery system [29–31]. We hypothesize this concept has a potential to be applied in the research field of mitigating FBR caused by implanted macroscopic biomaterials.

Liposomes have cell membrane structure and composition with phospholipid bilayer which are synthetic spherical vehicles enclosing an aqueous compartment and show excellent biocompatibility. As drug delivery systems, many liposomal formulations have been approved by the Food and Drug Administration (FDA) and widely applied in the clinic, including cancer therapeutics, fungal disease treatment, analgesics, photodynamic therapy, and viral vaccine delivery [32,33]. The primary building blocks of liposome are phosphocholine (PC) lipids. The zwitterionic headgroup of PC is known for its anti-protein adsorption property, and various artificially designed biocompatible coatings also use similar surface chemistry [34–36]. In addition to being a drug carrier, it is worth noting that liposomes have been found to have clinical effects on immunosuppression and anti-fibrosis. For example, Fotiadis et al. performed a midline laparotomy wound model in rat and showed that phospholipids reduced the secretion of local proinflammatory and profibrotic cytokines and inhibited fibrogenic properties of mesenchymal cells, which finally lead to the prevention of post-operative peritoneal adhesions [37]. La-Beck et al. also found that through decreased inflammatory factor interferon- γ (IFN- γ) expression by macrophages and cytotoxic T cells, liposomes can induce immunosuppression and improve angiogenesis [38,39].

In our previous work, we developed silk surface-functionalized electrospun fibers by single-component layer-by-layer (LbL) assembly and decorated the silk fibroin (SF) with IL-4 by click chemistry [40,41]. We found that these fibers with immunomodulatory ability can mitigate the FBR by regulating macrophage polarization in the early stage. However, the long-term release of IL-4 will cause local tissue fibrosis is still worthy of attention. In this study, we developed covalent bond mediated liposome fusion to construct “camouflage” coating to mitigate FBR and promote material-tissue integration. To prevent the interference caused by polymer degradation, we used bioinert polystyrene (PS) as a model polymer for electrospinning. Following the preparation of electrospun PS microfibrous scaffolds, SF-functionalized electrospun fibers by LbL deposition and then covalently modified with liposomes via copper-free strain-promoted azide–alkyne cycloaddition (SPAAC) click chemistry. We tested the hypothesis that the silk coating acts as a “bridge” to covalently immobilize liposomes and effectively mediate liposome fusion, forming a stable cell membrane-biomimetic lipid film (Fig. S1). Molecular dynamics simulations were used to theoretically analyze the interaction of liposomes physically adsorbed or click-bonded to the SF substrate. Importantly, the foreign-body responses to the liposome-decorated electrospun scaffolds in mice subcutaneous, including host cell infiltration, fibrotic tissue formation, inflammatory cell aggregation, angiogenesis, and macrophage

polarization, were investigated.

2. Results

2.1. Experimental design of liposome surface-modified electrospun PS fibers

We assembled a mixture of 1,2-dimyristoyl-sn-glycero-3-phosphatidylcholine (DMPC), 1,2-distearoyl-sn-glycero-3-phosphoethanolamine (DSPE), and cholesterol that mimicked the cell membrane’s physiologic components. Among them, DSPE has a clickable functional group N-dibenzocyclooctyne (DBCO) for further covalent surface modification of electrospun fibers (Fig. 1a, black box). Liposomes with a specific molar ratio of phospholipid composition (DMPC: DSPE: cholesterol = 78:2:20) were obtained by the thin layer evaporation (TLE) and extrusion through polycarbonate (PC) membranes (Fig. S2). The fabrication of liposome surface-modified nanofibrous scaffolds can be divided into 3 steps (Fig. 1a). The first step was to prepare polystyrene microfibrous scaffolds by electrospinning. Then the scaffolds were coated with SF or SF-azido via LbL self-assembly technique. The LbL deposition is mainly based on the driven forces of silk-silk hydrophobic interaction [40]. In the third step, the silk-coated PS microfibers were incubated with the click-functionalized liposome suspension at room temperature, and liposomes were physically adsorbed or covalently attached to the fibers, respectively. After that, PS fibers (Control), silk-coated fibers (Silk coating), liposomes physically adsorbed fibers (Adsorption) and click-covalently bonded fibers (Click) were implanted subcutaneously in mice to study the foreign-body reaction *in vivo* and related biological mechanisms (Fig. 1a, red box). In this study, we will investigate: ① Will “adsorption” and “click” cause liposomes to fuse and form lipid bilayers? ② Does the formed lipid film have fluidity? ③ Could “click” enhance the stability of lipid film *in vitro* and *in vivo*? and ④ Does the surface-modified liposome have a positive effect on the foreign-body reaction of the implanted electrospun scaffold? (Fig. 1b).

2.2. Characterization of clickable silk, liposomes, and LbL SF deposition

The covalent bonding between liposomes and SF-azido coating involved three procedures: diazonium coupling reaction, LbL coating and SPAAC click chemistry. Firstly, tyrosine residues in SF reacted with the diazonium introducing the azido groups into SF molecules (Fig. 2a, Step 1). To analyze the chemical bond and the conformational changes following this step, we examined the SF and SF-azido powder samples using Fourier transform infrared (FTIR) spectra (Fig. 2b). The characteristic peaks of the SF occurred at 1650 cm^{-1} (amide I) and 1532 cm^{-1} (amide II), which was consistent with previous studies [40]. For SF-azido, the characteristic peak at approximately 2124 cm^{-1} reflected the azido group, and the characteristic peaks at 1628 cm^{-1} and 1520 cm^{-1} indicated the formation of β -sheet structures. After the preparation of SF and SF-azido solution, the deposition of different numbers of SF layers was displayed using fluorescein isothiocyanate (FITC)-labelled SF during the LbL coating procedure (Fig. 2e). Confocal laser scanning microscopy (CLSM) images showed that the increase in numbers of coated layers resulted in the sufficient and uniform distribution of FITC-labelled SF on the surface of PS fibers. According to the quantitative fluorescence intensity of FITC-labelled SF, the scaffolds were adequately coated with SF after 5 layers of deposition, demonstrating that it is feasible to coat PS microfibrous scaffolds with SF via LbL assembly technique. The SF-azido reacted with the DBCO group in liposome forming the triazolyl via Cu-free SPAAC click reaction (Fig. 2a, Step 2). Zeta-potential measurements showed that liposomes were neutral and the addition of alkynyl rarely changed the charge (Fig. 2d). As characterized by dynamic light scattering (DLS), conventional liposomes tended to agglomerate into larger particles (341.7 nm), whereas alkyne-functionalized liposomes remained uniform particles (233.1 nm). To detect the azido-alkynyl bond, the SF, SF-azido solutions, and

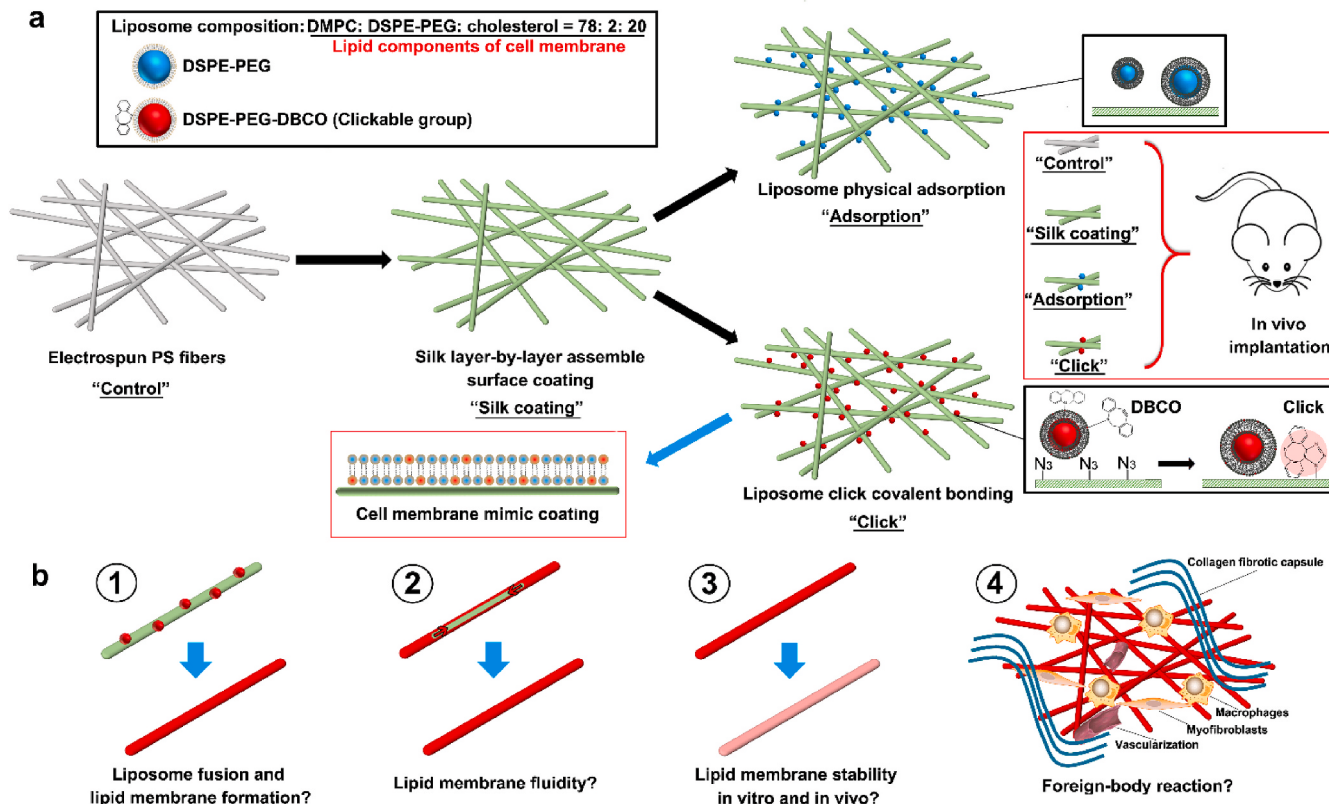


Fig. 1. Experimental design of liposome surface-modified electrospun PS fibers. (a) Schematic illustration of liposome surface-modified electrospun polystyrene (PS) fibers via physical adsorption and click chemistry. The experimental process involves preparing PS microfibrous scaffolds by electrospinning, coating silk fibroin as a “bridge” on the surface of electrospun fibers via layer-by-layer deposition, liposome surface-modified electrospun fibers via physical adsorption or click chemistry, and finally assessing the effect of this cell membrane biomimetic coating on the foreign-body reaction. (b) The main research issues of this study.

reaction mixture of SF-azido and fluorophore-alkynyl were analyzed using UV-Vis absorbance spectra from 225 to 500 nm (Fig. 2c). The diazonium coupling reaction with tyrosine residues in SF generated an absorption band at 352 nm, demonstrating that the reaction successfully attached the azido groups to the SF. Fluorophore-alkynyl was added into the SF-azido solution and the absorption band significantly weakened, indicating the formation of azido-alkynyl conjugates via click chemistry. For further evaluation of bonding efficiency, residual washing solutions were analyzed after the adsorption process or click reaction. SF-coated or SF-azido-coated fibers were immersed in the DBCO containing fluorescent probe (DBCO-PEG4-tetramethylrhodamine) solution. After reaction, we washed successively with ultrapure water and sodium dodecyl sulfate (SDS) solution to remove uncombined fluorophores (Fig. 2f). To compare the bonding efficiency, the residual washing solution was collected and measured using the fluorescence spectrophotometer. The fluorescence intensity of washing solution after click reaction was appreciably lower than that of washing solution after the adsorption method, indicating that more DBCO containing fluorescent probe were immobilized onto fibers via click chemistry.

2.3. “Click” surface modification to promote liposome fusion and maintain fluidity

As a cell membrane biomimetic coating, uniformity and fluidity are important physical properties of lipid bilayers, which can improve stability and provide subsequent embedding for functional proteins such as antibodies and cytokines [36,42,43]. Scanning electron microscope (SEM) images revealed the changes in the surface roughness of PS fibers after being coated with SF and liposome (Fig. 3a). Compared with control groups, multiple SF deposition made fibers obviously rough. The fibers decorated with liposomes exhibited different surface morphology.

Many particles unevenly distributed on the surface of fibers via physical adsorption. By contrast, the covalent binding possibly helped liposomes perform a stretched structure and the fibers tended to be much smoother. CLSM images also displayed the different surface distribution of liposomes on fibers (Fig. 3b). In the adsorption group, the liposomes remained particle morphology and dispersedly adsorbed on the surface of SF-coated fibers, while the liposomes immobilized on fibers via click chemistry evenly distributed. The high-resolution image of cross-section of liposome-decorated fibers was obtained by TEM (Fig. 3c). Larger particles were deposited on the fiber surface in the adsorption group. Conversely, a continuous distribution of small liposomes was discovered and a uniform lipid membrane was formed in the click group. As shown in Fig. 3d, electrospun PS microfibrous scaffold was hydrophobic and the water contact angle reduced from 117° to 87° after being coated with silk, which significantly improved the hydrophilicity of the PS scaffolds. For the electrospun fibers decorated with liposomes, the water droplets permeated immediately indicating their super hydrophilicity. The fluidity of lipid film on the fibers was investigated by fluorescence recovery after photobleaching (FRAP) experiments. After photo-bleaching, in both the adsorption group and the click group, surrounding fluorescent-labelled lipids moved to the photobleached black region and the red fibers were emerged again (Fig. 3e). The degree of recovery was evaluated by measuring the fluorescence intensity of the regions (Fig. 3f). In the adsorption group, the fluorescence intensity of recovery region gradually increased by 15% in 720 s. Likewise, the fluorescence intensity of fibers decorated with liposomes via click chemistry increased by 13%, which means the covalent conjugation slightly restricted the movement of lipids.

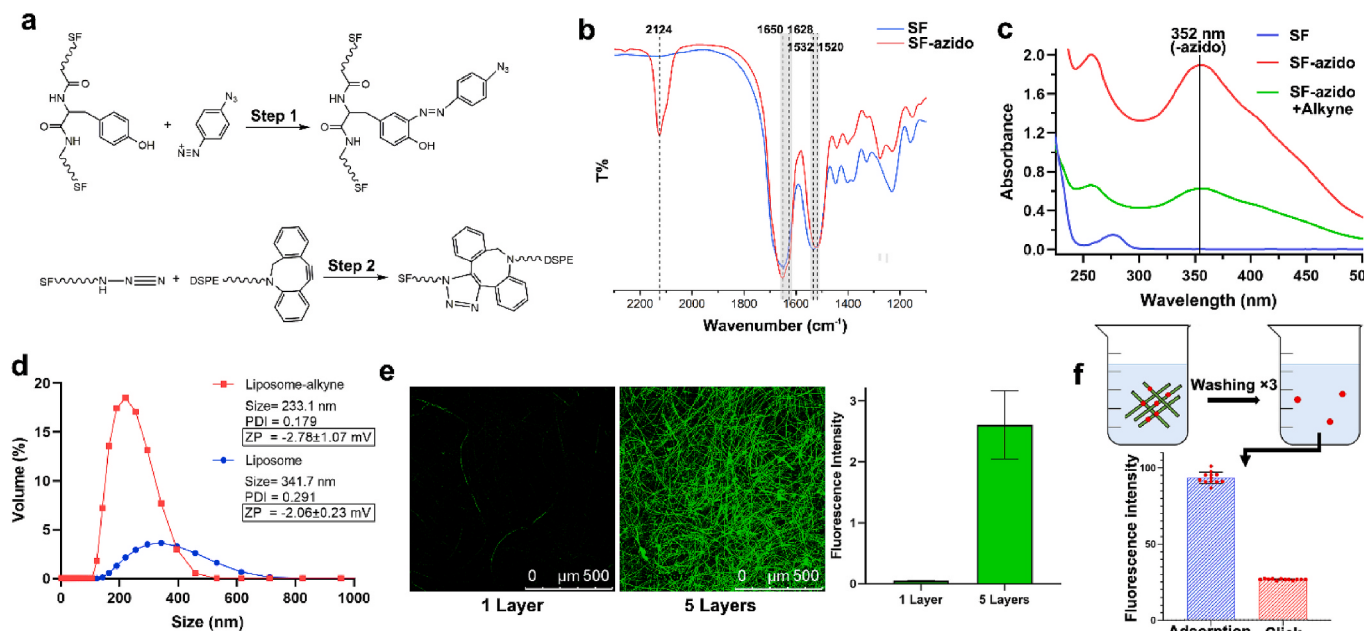


Fig. 2. Characterization of clickable silk, liposomes, and LbL SF deposition. (a) SF tyrosine diazonium coupling reaction introduces azide group (Step 1) and azido-functionalized SF connects DBCO of DSPE component in liposomes by copper-free SPAAC click chemistry (Step 2). (b) FTIR spectra of SF and azido-functionalized SF. (c) UV-Vis absorbance spectra of SF, azido-functionalized SF, and azido-functionalized SF after click chemistry from 225 to 500 nm. (d) Dynamic light scattering (DLS) analysis the size and zeta-potential of liposomes with clickable group and conventional liposomes. (e) Silk layer-by-layer deposition on the surface of electrospun PS fibers. Representative CLSM images of electrospun PS fibers with 1 layer and 5 layers of FITC-labelled SF (green) surface deposition and corresponding quantitative fluorescence intensity. Data are presented as the mean \pm SD ($n = 4$). (f) Click chemistry and nonspecific adsorption of the DBCO containing fluorescent probe on azido-functionalized SF coated electrospun scaffolds. Quantitative fluorescence density of the residual washing solution. Data are presented as the mean \pm SD ($n = 12$).

2.4. “Click” surface modification to improve liposome stability *in vitro* and *in vivo*

The stability of liposomes is an important parameter in clinical applications, wherefore we anticipate a covalent bond with the SF coating could prolong the retention time of liposomes *in vitro* and *in vivo*. We used CLSM and *in vivo* imaging system (IVIS) to detect the attenuation of the fluorescence intensity of RhB-labelled liposomes on the fiber surface to analyze the stability of liposomes *in vitro* and *in vivo* (Fig. 4). The electrospun fibrous scaffolds decorated with liposomes via different methods were incubated in PBS buffer at 37 °C for 7 days, and the solution was changed frequently. At first, both adsorption and click reaction produced the excessive accumulation of liposomes, or in other words, liposomes did not form lipid membranes on fibers in 6 h. After 24 h, the agglomerate particles negligibly decreased in the adsorption group, in contrast to the liposomes immobilized on fibers via click chemistry, which fused and turned into the lipid membranes. As shown in Fig. 4c, after 7 days incubation, although the liposomes partially fused, some particles still adhered to the surface of the fiber in the adsorption group. In contrast, the fiber surface still maintained a uniform lipid film in click group. We further analyzed the degradation of liposomes *in vitro* by detecting changes in fluorescence intensity (Fig. 4d). For physical adsorption, fluorescence intensity of liposomes declined to 30.50% of the initial value after 7 days of incubation, implying that most liposomes were lost or degraded. For click chemistry, the fluorescence intensity kept increasing in the first three days and reached a peak on the third day, which was consistent with the formation of the lipid membrane. The final fluorescence intensity was 52.39% of the maximum value in the click group after 7 days of incubation, significantly higher than that of the adsorption group. It seemed that click chemistry is beneficial for the even distribution of lipid layers on fibers and effectively reduces the loss of liposomes.

The *in vivo* stability of liposomes was investigated using IVIS (Fig. 4e and f). The living imaging of mice implanted with unlabeled scaffolds

did not show any fluorescent spots indicating that the interference from the autofluorescence of materials can be ignored. By measuring the fluorescence density, liposomes adsorbed to scaffolds were detected to degrade fast and hardly showed fluorescence signal after 14 days implantation. Liposomes click immobilized on scaffolds exhibited a higher fluorescence intensity and a slower downward trend. It is worth noting that after 7 days of implantation *in vivo*, it can be found that the fluorescence intensity decreased significantly in the “adsorption” group to 4.96%, and to 36.75% in the “click” group. Even after 14 days of implantation, the fluorescence intensity of the “click” group remained above 20% (23.2%). This phenomenon is consistent with the results of *in vitro* stability assessment.

2.5. Molecular dynamics simulation proves that “click” improves the binding rate and strength of liposome to silk substrate

In order to explain the rapid fusion in the click group, we conducted the MD simulations and displays the initial configuration of the liposome-SF system and the output configurations of 4 μ s MD simulation systems of physical adsorption and click chemistry (Fig. 5a). In a short time, DSPE-DBCO in liposomes can be tightly bound to the SF-azido coating through click chemistry, while liposomes without click group are still dissociated rather than adsorbed on the fiber. In the 4 μ s MD simulation system (Fig. 5b), click chemistry makes the contact frequency of liposomes and silk substrate increase rapidly with time. However, physical adsorption of liposomes does not increase the contact amount with SF. Therefore, a small amount of covalent bonding can make liposomes combine with the substrate more effective. The results indicated that click chemical covalent bonding can accelerate the immobilization of liposomes on the fiber and facilitate the fusion of liposomes into lipid bilayers.

In order to explain the stability of lipid membrane coating fibers via physical adsorption and click chemistry, we used MD to simulate the different interactions between the lipid membrane formed by liposome

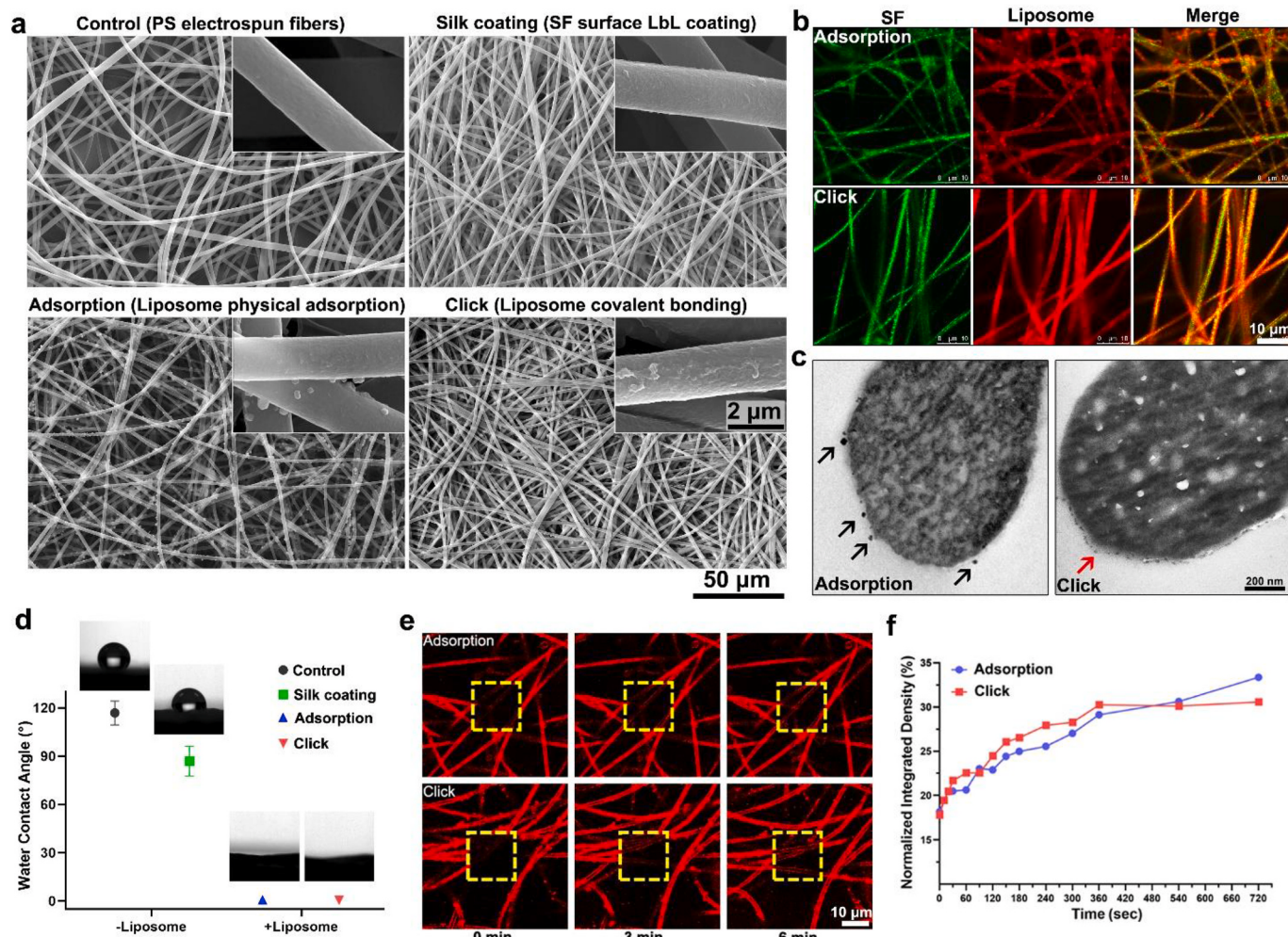


Fig. 3. “Click” surface modification to promote liposome fusion and maintain fluidity. (a) SEM images of the surface morphology of different electrospun fibers: “control” group (neat PS fibers), “silk coating” group (SF multilayers deposition on the surface of fibers), “adsorption” group (liposome-decorated fibers via physical adsorption), and “click” group (liposome-decorated fibers via covalent bonding). (b) Representative CLSM images were performed to observe the distribution of FITC-labelled SF (green) on PS fibers and RhB-labelled liposomes (red) on SF-coated fibers via “adsorption” and “click” group. (c) Representative TEM images were performed to observe the morphology and distribution of liposomes immobilizing onto SF-coated fibers via “adsorption” and “click”. The black arrow indicates physically adsorbed liposome particles, and the red arrow indicates covalently bound liposome fusion film. (d) Water contact angle of different scaffolds. Data are presented as the mean \pm SD ($n = 4$). (e) Fluorescence recovery after photobleaching (FRAP) of lipid film on the surface of fibers to analyze their fluidity. CLSM real-time observation of the fluidity of fluorescent-labelled lipid film (red) in “adsorption” and “click” group. The yellow box means the photobleaching region. Scale bars: 20 μm. (f) Fluorescence recovery percentage of the photobleached region of the “adsorption” and “click” fibers in 720 s.

fusion and the silk substrate. Both physical adsorption and covalent bonding can form continuous lipid film on SF coating (Fig. 5c). According to the time evolution of number of contacts between SF and lipid film (Fig. 5d), the contact frequency of click chemistry was obviously higher than that of physical adsorption over 4 μ s. Compared with physical adsorption, the binding energy (interaction energy) of click covalent bonding is increased by about 17 times. (Fig. 5e), indicating that the lipid film covalent bound to SF coating forms a more stable structure and would not exfoliate in a short time.

2.6. Histological observation of foreign-body reaction to liposome-functionalized electrospun fibers

Foreign-body reaction is an inevitable immune response when biomaterials implanted into the body, which determines functional retention and tissue integration of biomaterials. To identify the FBR of liposome-functionalized electrospun fibers, 4 groups of “Control”, “Silk coating”, “Adsorption”, and “Click” were implanted subcutaneously in BALB/c mice for 2 weeks. All the samples were subjected to

hematoxylin and eosin (H&E) and Masson’s trichrome staining (Fig. 6a and b). Compared with neat PS and silk coated scaffolds, the collagen fibrotic capsule was significantly decreased and the degree of cell infiltration was significantly increased in the both “adsorption” and “click” liposome-decorated scaffolds. According to the statistical analysis of the histological images, the decoration of liposomes significantly decreased the thickness of fibrotic capsules (Fig. 6c). Perhaps the LbL SF deposition on electrospun fibers reduced the connectivity of the pores to a certain extent, and the cell infiltration appeared to be significantly reduced in the “silk coating” group. However, after liposome surface functionalization, many host cells migrated into the scaffold again. This result indicates that liposomes can effectively promote host cell infiltration and accelerate the integration of tissue and scaffold (Fig. 6d). Importantly, the addition of liposomes effectively improved the number of new blood vessels inside the scaffold, which is a significant indicator of tissue healing and regeneration, and showed the good effect of tissue-material integration (Fig. 6e). In addition, the scaffolds decorated with liposomes displayed a small number of FBGCs formed at the material-tissue interface in comparison to the “control” group, but there was no

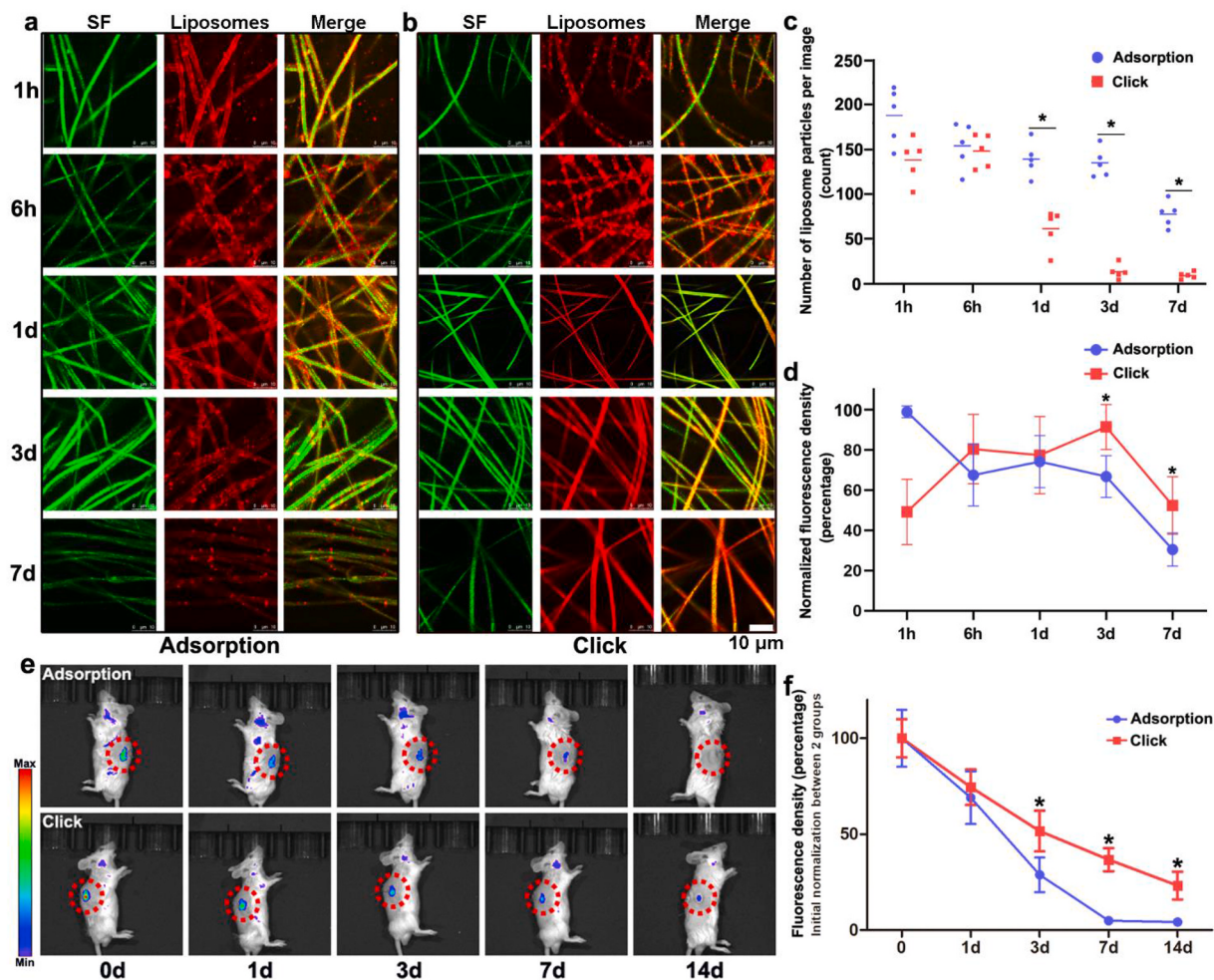


Fig. 4. “Click” surface modification to improve liposome stability *in vitro* and *in vivo*. Representative CLSM images of FITC-labelled SF (green) and RhB-labelled liposomes (red) on electrospun fibers via physical adsorption (a) and click chemistry (b) at various time points. Scale bars: 10 μm. (c) Counting the number of liposome particles on fibers per image. **p* < 0.05. Data are presented as the mean ± SD (*n* = 5). (d) Quantitative fluorescence intensity of liposomes on fibers at various time points. **p* < 0.05. Data are presented as the mean ± SD (*n* = 5). (e) High-sensitivity *in vivo* imaging of fluorescence of Balb/c mice subcutaneously implanted with fluorophore-labelled liposomes surface modified electrospun scaffolds at various time points. (f) Quantitative fluorescence intensity of fluorophore-labelled liposomes *in vivo* at various time points. **p* < 0.05. Data are presented as the mean ± SD (*n* = 4).

significant difference compared with the “silk coating” group (Fig. 6f).

2.7. Liposome-functionalized electrospun fibers reduce inflammation response and promote vascularization

To observe the short-term acute inflammation (7 days) and long-term vascularization (14 days) induced by different scaffolds in living animals in real-time, we used relevant fluorescent imaging probes targeting inflammation and neovascularization for *in vivo* imaging (Fig. 7a). The radiant efficiency of cathepsin B protease-activated probe (ProSense 750) reflected the early inflammatory cell responses (Fig. 7b and c). In the first 3 days of scaffold implantation, there was no significant difference in the inflammatory cell response caused by different groups. However, we found that after 7 days of implantation, the probe fluorescence intensity of the liposome-decorated scaffolds was significantly reduced compared to the “control” and “silk coating” groups. The radiant efficiency of integrin $\alpha_5\beta_3$ -activated probe (IntegriSense 645) reflected neovascularization (Fig. 7d and e). The fluorescence intensity of SF coated scaffolds was similar to that of PS scaffolds. However, the fluorescence intensity of liposome-decorated scaffolds was significantly higher in 3, 7, and 14 days, which indicated that liposomes were beneficial to the formation of new blood vessels. Myofibroblasts, as inflammatory cells, have been shown to play an important role in tissue

fibrosis and the FBR, and have been used as a representative cell type to analyze the degree of inflammation. After 14 days of implantation, we performed immunofluorescence observation on tissue sections and found that compared with the “control” and the “silk coating” groups, the number of α -SMA-positive myofibroblasts was significantly reduced on the liposome-decorated scaffolds (Fig. 7f). However, the number of CD31-positive cells representing neovascular endothelial cells was greatly increased on the liposome-decorated scaffolds, especially the “click” group (Fig. 7g).

2.8. Liposome-functionalized electrospun fibers promote macrophage polarization toward a pro-regenerative phenotype

In the process of tissue repair and material implantation, the differentiation of myofibroblasts and the production of new blood vessels are mainly regulated by immune cells, especially macrophages [44,45]. The ratio of M1 pro-inflammatory and M2 pro-regenerative macrophages in the material implantation *in situ* can reflect the different stages of wound healing and the degree of FBR [8]. To determine whether liposomes mitigate FBR by regulating macrophage phenotype, we used continuous sections for immunofluorescence detection of M1 (CCR7) and M2 (CD206) surface markers of macrophages, following the subcutaneous implantation for 14 days (Fig. 8a). We found that compared with the

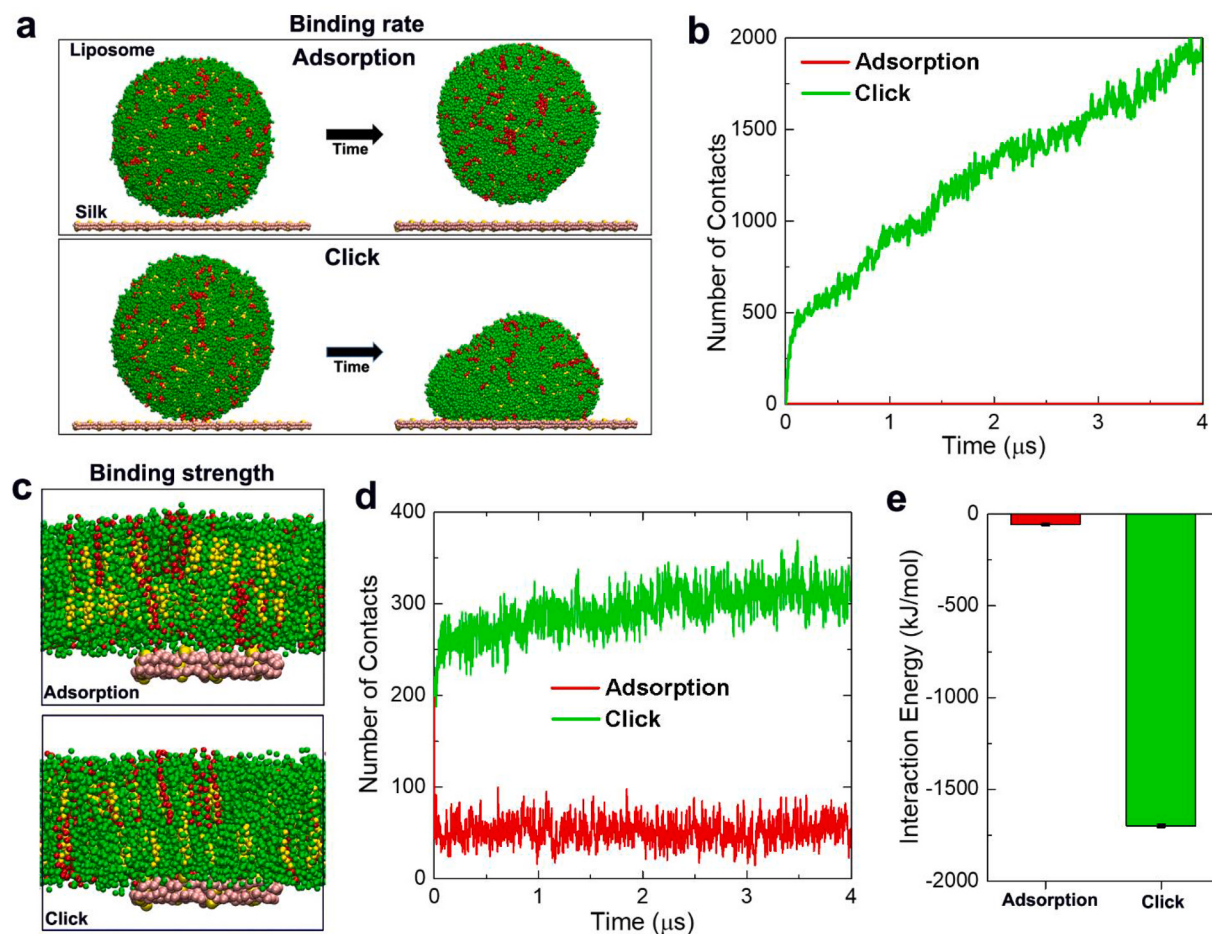


Fig. 5. Molecular dynamics simulation proves that "click" improves the binding rate and strength of liposome to silk substrate. (a) Snapshots for the initial configuration of liposome-SF system and the output configurations of 4 μ s MD simulations in "physical adsorption" and "click chemistry" cases. (b) Time evolution of the number of contacts between SF and liposome. (c) Last frame snapshots of simulation systems of physical adsorption and click chemistry. (d) Time evolution of the number of contacts between SF and DMPC/DSPE/CHOL membrane. (e) Interaction energy between SF and DMPC/DSPE/CHOL membrane. DMPC: green, DSPE: red, CHOL: yellow; SF: pink & yellow. Mean \pm SD was used based on the five-block average over the last 1 μ s MD trajectories.

"control" and "silk coating" group, the proportion of CCR7-positive macrophages decreased significantly in liposome-decorated scaffolds. On the contrary, the proportion of CD206-positive macrophages increased significantly. It is worth noting that the "click" group expressed more CD206-positive macrophages inside the scaffold than the "adsorption" group, which may be related to the high *in vivo* stability of the covalent bond (Fig. 8b). This result demonstrates that liposome-decorated scaffolds can effectively increase the ratio of M2/M1 *in vivo*, especially the covalently bound liposomes potentially promote macrophage polarization toward M2 type.

3. Discussion

Liposomes are recognized as an important drug delivery vehicle with attractive properties, such as cell membrane biomimetic structure and excellent biocompatibility. Liposomal encapsulation of drugs can reduce drug toxicity and extend duration of therapeutic effect. The liposome encapsulation of hydrophilic and hydrophobic small molecule therapeutic agents and other biomacromolecules has been established [46–49]. So far, FDA-approved liposome-based therapies involve a wide range of applications in anti-cancer, antibacterial and antiviral treatments [34]. Utilizing the drug encapsulation and delivery capabilities of liposomes, combined with the scaffold materials that provide physical support and a cell-friendly microenvironment, can effectively improve the local drug concentration and controlled-release ability, and enhance

the therapeutic effect of the scaffolds. It has great clinical application potential in the fields of antibacterial dressings, implants, and regenerative medicine [32]. Electrospun micro/nano fibrous scaffolds have the characteristics of similar extracellular matrix fibrous structure and high specific surface area, and they are excellent candidates as scaffold materials that can be decorated by liposomes. For example, Monteiro et al. covalently immobilized gentamicin-loaded liposomes on the surface of electrospun nanofibers through the thiol-maleimide reaction, which enhanced the sustained drug release performance and enhanced the antibacterial performance as a skin wound dressing [50]. Chandrawati et al. modified the surface of liposomes loaded with enzyme pro-drug- β -glucuronidase on PVA electrospun fibers, which can achieve long-term drug release performance and maintain enzyme bioactivity [51]. Recently, Xi et al. covalently bound the liposome loaded with IL-4 plasmid DNA to the surface of electrospun nerve guide conduit through a condensation reaction, so that it has the immunomodulatory ability to regulate the macrophage polarization, and then promote the functional recovery of nerve tissue [52]. These studies have achieved good results, but the fusion, fluidity, stability, and inherent biological response of the decorated liposomes still need to be further explored.

This study used liposomes with the same basic components as natural cell membranes, and compared the physicochemical properties and biological responses of liposomes modified electrospun fibers by physical adsorption and covalent modification (SPAAC click chemistry). Due to the modifiable sites and excellent stability of SF molecules, the silk

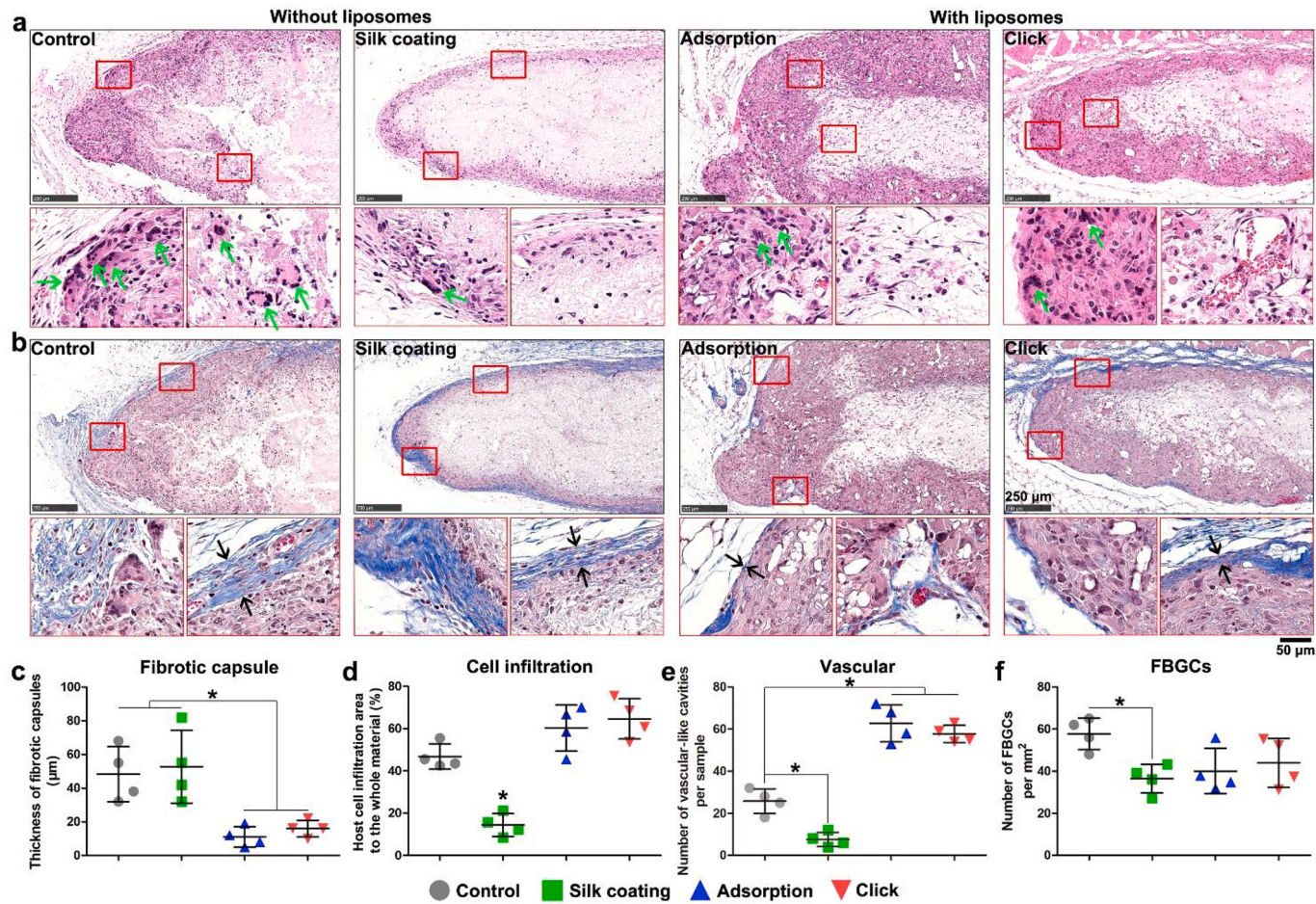


Fig. 6. Histological observation of foreign-body reaction to liposome-functionalized electrospun fibers. Representative H&E (a) and Masson's Trichrome staining images (b) of histological sections of different scaffolds after 14 days of subcutaneous implantation. The green arrows indicate FBGCs and the black arrows indicate fibrotic capsules. Statistical analysis of the thickness of fibrotic capsules (c), the number of host cells infiltration (d), the number of blood vessels (e), and the number of FBGCs surrounding the implanted scaffolds (f). * $p < 0.05$. Data are presented as the mean = SD ($n = 4$).

layer-by-layer assembly surface coating can be used as a ‘bridge’ to connect functional macromolecules [41]. Compared with the existing electrospun fiber surface modification technologies, our method has certain advantages and limitations. At present, the main surface modification methods of electrospun fibers are traditional LbL self-assembly, plasma irradiation, and surface chemical treatment [53]. The traditional LbL assembly technique enables the deposition of ultrathin and uniform films by the sequential electrostatic deposition of oppositely charged polymers. Electrostatic forces generally drive the deposition on charged components, but in our study, the single-component LbL coating established by hydrophobic interaction of silk can avoid the inherent biological toxicity of positively charged polymers. Plasma irradiation treatment uses highly oxidized charged ions generated by the ionization of gases such as oxygen, nitrogen, and ammonia under the action of an electric field, which can bind to the surface of electrospun fibers to form functional groups. Because electrospun scaffolds are high-density porous fibrous scaffolds, it is difficult for plasma to enter the inside of scaffolds, thus affecting the modification effect. However, high energy plasma irradiation will increase the local temperature, which will change the morphology and mechanical properties of the electrospun fibers. Similarly, chemical surface treatment, such as aminolysis and alkali treatment, often involves change in pH value and temperature by soaking in solution, which often leads to the change of fiber structure and the decrease of mechanical properties. The silk coating in this study also has multiple-steps and time-consuming operations. Because it uses the principle of hydrophobic interaction, it can only be used on

hydrophobic polymer surfaces. In the future, we need to improve the operation efficiency and application scope of the silk coating by modifying the SF molecules, such as changing the side chain charge and molecular conformation (β -sheet content increases hydrophobic interaction).

The results of SEM, CLSM, and TEM showed that both physical adsorption and covalent binding of liposomes can be effectively attached to the surface of the fiber coated with SF. However, the liposomes in the physical adsorption group showed dispersed particles on the fiber surface, and the use of click chemistry covalent immobilization could make the liposomes quickly form a uniform surface coating similar to cell membrane, indicating that covalent binding is conducive to the rapid fusion of liposomes to form lipid membrane. In the *in vitro* degradation process, it was found that compared with physical adsorption, the liposomes of the click group showed obvious rapid fusion and formed a uniform lipid film. In contrast, the liposomes of the physical adsorption group still had a large number of particles. With the extension of the degradation time, it was found that the fluorescence intensity reduction rate in the physical adsorption group was significantly faster than that of the clicked liposomes, indicating that click covalent binding can effectively improve the stability of the liposome coating. The real-time observation of the stability in mice by the IVIS found that the trend of fluorescence decline has a similar result. Pasquardini et al. deposited liposomes on a flat substrate by electrostatic interaction and covalent bonding, and found that compared with electrostatic adsorption, the stability of the covalently immobilized lipid membrane was

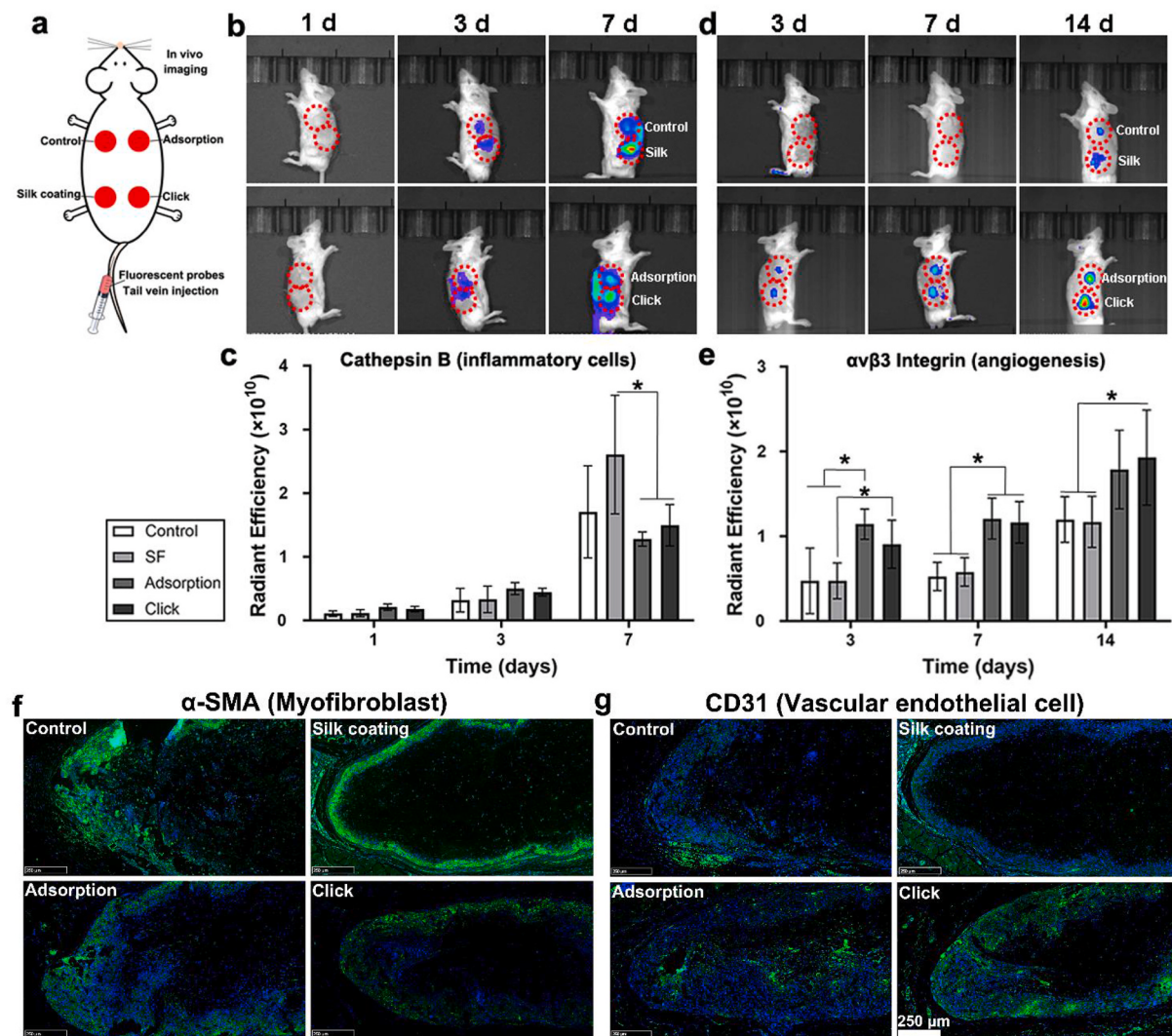


Fig. 7. Liposome-functionalized electrospun fibers reduce inflammation response and promote vascularization. (a) The schematic diagram shows that different scaffolds were implanted subcutaneously in mice, and the *in vivo* imaging was performed with fluorescent probes related to inflammation and vascularization. (b) High-sensitivity *in vivo* imaging of fluorescence of the cathepsin B protease-activated probe (ProSense 750) of different scaffolds implanted subcutaneously in mice for 1, 3 and 7 days. (c) Quantitative radiant efficiency of ProSense 750 at various time points. * $p < 0.05$. Data are presented as the mean \pm SD ($n = 4$). (d) *In vivo* imaging of fluorescence of the integrin $\alpha_v\beta_3$ -activated probe (IntegriSense 645) of different scaffolds implanted subcutaneously in mice for 3, 7 and 14 days. (e) Quantitative radiant efficiency of IntegriSense 645 at various time points. * $p < 0.05$. Data are presented as the mean \pm SD ($n = 4$). (f) and (g) α -SMA and CD31 immunofluorescent staining of histological sections of different scaffolds after 14 days subcutaneous implantation, respectively. The images show the number and distribution of myofibroblasts and vascular endothelial cells on different scaffolds.

increased by about ten times [54]. Furthermore, we analyzed the binding rate and strength of liposomes and silk substrates through molecular dynamics simulations, and theoretically clarified the difference between physical adsorption and covalent binding. At the same time, the contact frequency between the liposome with click group and silk fibroin coating was much higher than that of physical adsorption, which made the liposome combine with silk substrate more quickly. Most of the liposomes were immobilized by chemical bonds, and then fused with each other to form a lipid membrane. However, the liposomes without chemical bond attraction were still in free state for a long time and needed longer reaction time to adsorb on the fiber surface. In addition, FRAP experiments proved that although the covalently bound liposomes increased stability, they still formed a lipid bilayer with fluidity. As dynamic biomaterials provide lateral fluidity and cell membrane-like environments, which can effectively embed functional proteins such as antibodies and cytokines to achieve selective targeting of cells [36,42].

Lipid membrane can be used to simulate the physicochemical and biological properties of cell membrane, which can modify the surface of

implanted biomaterials and construct "camouflage" coating to improve the biological tolerance. Researchers modified the surface of organic and inorganic nanoparticles with lipid membranes to increase the circulation time of drug-carrying particles *in vivo*. Functionalized liposome coatings make these nanoparticles have invisible properties in the blood [29,30,33]. At present, most researches mainly focus on the development and application of lipid membrane-encapsulated particle drug delivery system. In this study, because covalent-bonding facilitates the fusion of liposomes to form a solid-supported lipid bilayer, we verified the *in vivo* host response of this "camouflage" surface coating technology to the bulk electrospun fiber scaffold. In a mouse model of subcutaneous implantation, histological observation showed that the surface of the liposome-modified electrospun fibrous scaffold can effectively increase host cell infiltration and reduce the formation of fibrous capsules. Importantly, it can significantly improve the angiogenesis inside the scaffold. We found that both physical adsorption and covalent bonding, the cell-like membrane coating can effectively mitigate the FBR caused by the implantation of the electrospun scaffold. Since the PC headgroup

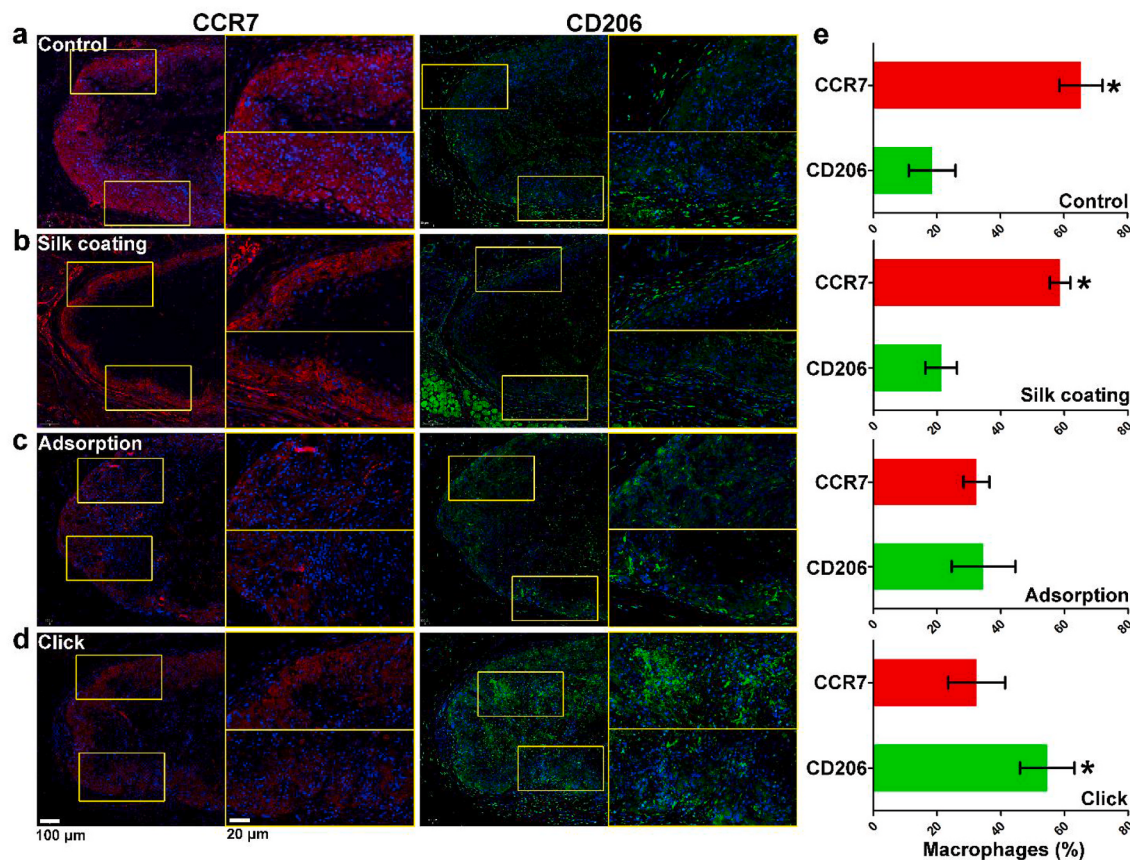


Fig. 8. Liposome-functionalized electrospun fibers promote macrophage polarization toward a pro-regenerative phenotype. (a–d) Immunofluorescent images of macrophages stained with pro-inflammation phenotype markers CCR7 (red), anti-inflammation phenotype markers CD206 (green) and DAPI for nuclei on continuous sections of different scaffolds. (e) Analysis of the Arg-1⁺/CCR7⁺ ratio of histological sections of different scaffolds after 14 days of subcutaneous implantation. * $p < 0.05$. Data are presented as the mean \pm SD ($n = 8$).

is a zwitterionic polymer, it has a net charge of zero and is heavily hydrated [35]. The lipid membrane surface coating can form a hydration layer on the surface of the material, which can effectively reduce non-specific protein adsorption, thereby reducing the initial aggregation of inflammatory cells. Real-time observation of functional probes *in vivo* imaging and immunofluorescence results showed that the expression of proteases related to inflammatory cells decreased, the number of myofibroblasts decreased, and the increase of angiogenesis indicated that there were obvious characteristics of the wound healing process in the liposome-modified scaffold [44].

2-methacryloyloxyethyl phosphorylcholine (MPC), as a zwitterionic polymer that mimics natural cell membranes, can be effectively used for surface modification of implant biomaterials to improve biocompatibility and hemocompatibility. In addition, its zwitterionic structure can produce a hydrated isolation layer on the surface, which has lubricating properties and anti-protein and cell adhesion capabilities *in vivo* [55,56]. Non-specific protein adsorption is an important factor to determine the degree of FBR. Recently, it has been reported that covalently bonding MPC to the surface of polydimethylsiloxane (PDMS) can significantly reduce the thickness of fibrous capsule and inflammatory markers produced by long-term FBR [57]. At the same time, compared with natural phospholipids, due to the inherent excellent stability of MPC, it can effectively increase the residence time *in vivo* [58,59]. However, the liposome surface modification in this study has the following advantages compared to MPC: (i) Liposomes, as drug carriers, can combine the encapsulation and delivery of small molecule drugs, genes, and functional proteins to increase the functional diversity of implanted scaffolds; (ii) The lipid membrane formed by liposome surface coating has fluidity and similar physical properties to natural cell membrane. It can

be embedded functional proteins such as cell surface receptors or ligands to increase the biological functions of the coating; (iii) The composition of liposomes has a variety of selectivity, and the composition of liposomes can be changed according to the needs. For example, the anti-inflammatory components such as phosphatidylserine or sphingosine 1-phosphate can be added instead of DMPC [60–63]; (iv) It has been found in clinical practice that liposomes themselves have immunoregulatory functions such as reducing postoperative tissue adhesion and promoting angiogenesis [37,39]. In addition, the SPAAC click chemistry technology used in this study to covalently bond the liposomes with the substrate material effectively improves the stability of the liposomes *in vivo* and reduces the limitations of natural phospholipid coatings. In summary, compared with MPC, liposome functional coating can not only provide an inert surface to reduce protein adsorption and FBR, but also has great potential in tissue regeneration, anti-tissue adhesion, and drug delivery.

We further analyzed the macrophage polarization, an important immune regulatory cell in wound healing, and observed the expression of pro-inflammatory and pro-regenerative macrophages inside the scaffold. Activated macrophages have been classified as different subtypes, during the innate immune response and inflammation by the invasion of foreign implants, inflammatory cytokines such as tumor necrosis factor (TNF) and interferon gamma (IFN- γ) activate macrophages as pro-inflammatory M1 phenotype, which are implicated in phagocytosis and initiating inflammation. By contrast, activation by IL-4 or IL-13 polarizes macrophages as anti-inflammatory M2 macrophages, which have pro-regenerative properties and are involved in tissue homoeostasis [64,65]. Compared with the “control” group and “SF coating” group, the proportion of M1 macrophages was significantly

reduced after the scaffold was modified with liposomes. It is worth noting that the liposomes in the “click” group have better stability *in vivo*, promote the proportion of macrophages to M2 polarization, and finally improve the material-tissue integration and angiogenesis. Clinical trials have found that despite the pharmacological advantages of improved drug delivery, liposome-mediated therapies have largely failed to increase anticancer efficacy over conventional formulations [66]. Sabnani et al. found that liposomes themselves have immunosuppressive and angiogenesis effects, similar to that used in patients, directly counterbalancing their anti-cancer activity [38]. Therefore, liposomes may have a similar biological mechanism in wound healing, mainly by regulating the macrophage polarization to reduce the innate inflammatory response and improve the angiogenesis effect, thereby promoting the integration of materials and surrounding tissues and mitigating the foreign-body reaction caused by implantation.

In this study, our liposome surface-modified electrospun scaffold with anti-FBR function may have application prospects in the following fields: (i) Tissue repair patch: The soft tissue repair patch as a physical support needs a good ability to promote tissue regeneration. The liposome surface-modified electrospun scaffold can promote host cell infiltration and strengthen the integration of tissue/scaffold. Importantly, a high degree of vascularization can increase the transport and exchange of nutrients and metabolites at the repair site and enhance the tissue repair and regeneration capabilities. (ii) Post-operative anti-adhesion barrier: In the process of soft tissue repair after surgery, the accumulation, proliferation, and differentiation of fibroblasts and myofibroblasts lead to excessive deposition of collagen, and the resulting fibrotic tissue will cause adhesion between the injured site and peripheral tissue. In clinical practice, polymer membrane barriers are often used to block the injury site and peripheral tissue. This liposome surface-modified electrospun scaffold can reduce the expression of myofibroblasts and the secretion of collagen by regulating the macrophage polarization, and lower fibrosis can effectively prevent tissue adhesion; (iii) *In situ* drug delivery system: In clinic, it is often necessary to keep high concentration of drugs in local area for a long time, such as repairing damaged tissue or releasing anticancer drugs in tumor resection site. In this study, liposome can be used as “microcarriers” of drugs for encapsulation and release, while electrospun scaffold can be used as “macroaggregates” to enhance *in situ* drug delivery.

4. Conclusion

In summary, we have developed a cell membrane-biomimetic coating formed by click-mediated liposomes immobilization and fusion on the surface of electrospun fibers. This kind of lipid film not only maintained good uniformity and fluidity, but also improved the stability *in vitro* and *in vivo* compared with physical adsorption. Molecular dynamics simulations clearly explained that the rapid immobilization and fusion of click-mediated lipid films is mainly due to the increase in the bonding rate and strength of liposomes to the silk substrate. Significantly, the liposome surface functionalization promoted host cell infiltration and reduced the thickness of fibrotic capsules, improving vascularization and the integration of the tissue and scaffold. The biological mechanism of these functions may be closely related to macrophages polarize toward a pro-regenerative phenotype. The present study offers a new approach for micro-nanofibers surface modification, which not only as anti-FBR coatings but also as cell membrane-biomimetic substrate with interesting possible applications such as tissue repair patch, post-operative anti-adhesion barrier, or *in situ* drug delivery system.

5. Materials and methods

5.1. Electrospinning

PS nanofibrous scaffolds were fabricated by electrospinning. PS (Mw

= 280,000, Sigma, USA) was dissolved in a N,N-Dimethylformamide (DMF, 99.8%, Mw = 73.09) solution with a final concentration of 30% (w/v). To spin the PS solution, an 18 kV high voltage was applied to the needle of the syringe and a piece of tinfoil was used as a grounded collector.

5.2. Preparation of SF solution

To prepare the aqueous SF solution, pieces of silkworm cocoon was boiled twice in the boiled aqueous solution of 0.02 M Na₂CO₃ for 1 h and rinsed 3 times with ultrapure water. Subsequently, it was boiled in ultrapure water for 10 min, rinsed 5 times and dried in a fume hood for a night. The degummed SF was dissolved in 10 M LiBr (Mw = 86.85, Sigma) by stirring for 1 h and heating up to 65 °C for 2 h. To remove the remaining impurities, the solution was filtered through a 0.45 µm syringe filter and dialyzed (MWCO = 3500 Da, Viskase, USA) against ultrapure water for 3 days. The final SF solution was stored at 4 °C with a concentration of 5% (w/v).

5.3. Preparation of FITC-labelled SF

The FITC-labelled SF was prepared using EDC/NHS chemistry. Firstly, 80 mg 1-Ethyl-3-(3-dimethylaminopropyl) carbodiimide hydrochloride (EDC, Mw = 191.70, Thermo, USA) and 220 mg N-hydroxysuccinimide (NHS, Mw = 115.09, Thermo) were blended in 10 mL of a 2% (w/v) SF solution dialyzed against MES (Mw = 213.20, Solarbio) buffer (pH = 5.6). The activation of the carboxyl groups of SF was terminated after 15 min by β-mercaptopropanoic acid (Sigma), followed by the addition of ethylenediamine (Sigma) to stir for 2 h. The solution was then dialyzed against MES buffer for 12 h and reacted with 10 mg Fluorescein-5-isothiocyanate (FITC, Mw = 389.38, Sigma) for 2 h. Finally, the solution was dialyzed against ultrapure water for 24 h and filtered through a 0.45 µm syringe filter, yielding a FITC-labelled SF with a concentration of approximate 1% (w/v).

5.4. Preparation of azido-functionalized SF

The azido-functionalized SF was prepared by a diazonium coupling reaction with tyrosine residues in SF as previously reported [67]. Briefly, 4-azidoaniline hydrochloride (0.360 mmol, Mw = 170.60, Sigma) was dissolved in 1 mL of a 1:1 acetonitrile/water solution, which was then mixed with 0.5 mL of a p-toluenesulfonic acid (1.430 mmol, Mw = 190.22, Sigma) aqueous solution. Subsequently, the solution was blended with 0.5 mL of a sodium nitrite (0.715 mmol, Mw = 69.00, Sigma) aqueous solution and stirred at room temperature for 15 min. All the solutions were prepared in an ice bath before mixture. The diazonium coupling reaction was started by adding 10 mL of a 5% (w/v) borate-buffered SF solution (pH = 9) into the diazonium salt solution. The reaction was proceeded in the ice bath for 30 min, followed by the dialysis against ultrapure water for 24 h.

5.5. SF LbL surface deposition

With the purpose of surface modification, the PS nanofibrous scaffolds were cut into 1 cm × 1 cm × 100 µm square shape and incubated with 0.05% (w/v) polyethyleneimine (PEI, Mw = 25,000, Sigma) for 15 min. After being washed, the nanofibers were incubated with 0.1% (w/v) SF solution at 4 °C for 15 min and washed 3 times with ultrapure water. The SF-coated PS nanofibers were immersed in 90% methanol (Mw = 32.04, BOYUAN) for 15 min to form silk crystalline β-sheets. The nanofibers were dried under nitrogen gas and subjected to the next coating procedure until the desired number of layers was deposited.

5.6. Preparation of liposomes and rhodamine B -labelled liposomes

To prepare liposomes, the lipid stock solutions were added into a

reagent bottle and comprised of 20 mol% cholesterol ($M_w = 386.65$, Avanti, USA), 2 mol% 1,2-distearoyl-sn-glycero-3-phosphoethanolamine-N-[dibenzocyclooctyl(polyethylene glycol)-2000] (DSPE-PEG (2000)-DBCO, $M_w = 3077.80$, Avanti) and 78 mol% 1,2-dimyristoyl-sn-glycero-3-phosphatidylcholine (DMPC, $M_w = 677.93$, Avanti). After evaporation of chloroform under nitrogen gas, the lipid film was dissolved in 5 mL of PBS buffer ($pH = 7.2\text{--}7.4$, Solarbio) at 75°C until all lipids were mixed. The suspension was subjected to freeze-thaw cycles 3 times and extruded through the 0.2 μm PC membrane (Whatman) by a mini extrusion (Avestin, Canada) to form lipid vesicles. The resultant vesicle solution was stored at 4°C until usage. RhB-labelled liposomes were made by replacing 1 mol% DSPE with 1,2-dioleoyl-sn-glycero-3-phosphoethanolamine-N-(lissamine rhodamine B sulfonyl) (RhB-DSPE, $M_w = 1301.715$, Avanti).

5.7. Liposome surface-modified electrospun fiber via click chemistry

Liposomes were combined with the surface-modified PS nanofibrous scaffolds via physical adsorption or strain-promoted azide-alkyne cycloaddition (SPAAC) click chemistry. In brief, azido-SF coated electrospun scaffolds were incubated with liposome or DBCO-functionalized liposome suspension at room temperature for 72 h, respectively. After incubation, the scaffolds were washed 3 times with PBS buffer and the uncombined liposomes were washed away.

5.8. Characterizations of SF, azido-SF, and liposome

Chemical and structural analyses of freeze-dried samples prepared from SF and SF-azido were measured by Fourier transform infrared spectroscopy (FTIR) over a wavenumber range from 4000 to 400 cm^{-1} . The FTIR spectra of different samples were obtained by a Nicolet spectrometer system (System 2000, PerkinElmer) with a DTGS KBr detector. Chemical analyses of SF and SF-azido solutions were performed on the UV-Vis spectrometer (ThermoFisher, USA) over a wavenumber range from 200 nm to 550 nm. The efficiency of the diazonium coupling reaction and click chemistry were assessed by UV absorbance at 352 nm. Dynamic light scattering (DLS) was performed on a Malvern Zetasizer Nano ZS (Malvern, Germany) to characterize the size and zeta potential of liposomes. Samples were prepared by diluting 1 mL liposome solution with 19 mL PBS buffer and sonicating. Particle size and surface charge were measured at 25°C by using a standard operating procedure. To evaluate the reaction efficiency of DBCO group and azido-SF surface-modified electrospun microfiber, DBCO-PEG4-tetramethyl-rhodamine B ($M_w = 936.06$, Sigma), as a substitute, was dissolved in ultrapure water and reacted with fibers by shaking at room temperature. After being washed, the fibers were observed using a CLSM and the fluorescence intensity of the residual washing solution was measured by fluorescence spectrophotometer (ThermoFisher, USA).

5.9. Characterization of liposome-functionalized electrospun scaffolds

The morphology of PS, SF coating, liposome-functionalized electrospun scaffolds was characterized using a scanning electron microscope (SEM, Zeiss, Germany) after the samples were coated with gold. Fluorescence images of liposome-adsorbed or -clicked electrospun scaffolds were obtained using a confocal laser scanning microscope (CLSM, Leica, Germany) and quantitative fluorescence intensity was analyzed by ImageJ. To observe the high-resolution fiber cross section, a transmission electron microscope (TEM, FEI, Netherlands) was employed. Liposome-decorated fibers were embedded in paraffin and sectioned into 10-nm-thick slices before placed on a copper grid. All TEM images were performed at 100 kV. The hydrophilicity of scaffolds was determined by water contact angle (JC2000FM, Powereach, China) measurements. To examine the fluidity of lipid film on scaffolds, fluorescence recovery after photobleaching (FRAP) experiments were carried out using a CLSM. The scaffolds were decorated with RhB-

labelled liposomes via physical adsorption or click chemistry and images were taken before photobleaching at 1% of maximum laser power. Photobleaching was performed at 50% of maximum laser power and the area was selected by the zoom control of the instrument. Afterwards, the fluorescence recovery was monitored by capturing images every 10 s at 1% of maximum laser power and the data were quantitated using ImageJ densitometry analysis.

5.10. In vitro evaluation of the stability of liposome-functionalized fibers

The distribution and *in vitro* degradation of liposomes on electrospun scaffolds were observed by CLSM using the fluorescent marker. RhB-labelled liposomes (red) were immobilized on fibers through physical adsorption or click chemistry. The prepared scaffolds were immersed in PBS buffer at 37°C for 7 days and the buffer was changed frequently. The *in vitro* stability of liposomes was observed by CLSM and the changes in fluorescence density were analyzed by ImageJ.

5.11. Molecular dynamics (MD) simulation

MD simulations have been proven to be a powerful tool in studying the interface between materials and biological systems. In this work, Martini coarse-grained (CG) force field (version 2.1) were used to capture the adsorption dynamics of lipid vesicle onto the silk fibroin interface [68,69]. The peptide GAGAGS, whose atomic structure was adapted from Patel's work [70], was firstly converted into Martini model and then evenly distributed in x/y plane to achieve two planar silk fibroin interfaces ($12\text{ nm} \times 12\text{ nm}$ and $35\text{ nm} \times 35\text{ nm}$). Both the planar lipid bilayer and lipid vesicle (DPPC: DSPE: cholesterol = 70: 10: 20) was placed on these two silk fibroin interfaces respectively. Additional strong attractive interaction potential was applied to the DSPE head-group and peptide sidechains to mimic the "click chemistry" effects between DSPE and silk fibroin. The planar lipid bilayer consists of 504 DPPC, 72 DSPE and 144 cholesterols, while the lipid vesicle contains 2577 DPPC, 368 DSPE and 736 cholesterols, which was built using CHARMM-GUI [71]. For all simulations, GROMACS software (version 2016.5) and suggested parameters were used. Each simulation was run for 1 μs with the time step of 20 fs.

5.12. Subcutaneous implantation

Male BALB/c mice, weighing 20–23 g, were raised in a mouse feeding system regarding the Guiding Principles for the Care and Use of Animals of Beihang University and was approved by the Biology and Medical Ethics Committee of Beihang University (Approval number: BM20180041). The scaffolds were cut and folded into $1\text{ cm} \times 1\text{ cm} \times 0.2\text{ mm}$ ($L \times W \times T$) shapes after sterilization. All the mice were anesthetized with 0.5% pentobarbital sodium. Two small midline incisions were made on the dorsum of each mouse, and the scaffolds were introduced in lateral subcutaneous pockets created by blunt dissection. Procaine penicillin (20 mg/kg) was given intramuscularly preoperatively and after the operation for prophylactic infection control. Both animals remained in good general health throughout the study, as assessed by their weight gain. After 14 days, the rats were sacrificed, and the implanted scaffolds were removed en-bloc with the naturally surrounding tissue. The samples were fixed and processed for histology, as described below. Four replicates of each type of electrospun scaffolds were implanted into four different rats to provide statistical significance in the histological studies.

5.13. In vivo imaging

A small animal optical *in vivo* imaging system (IVIS, PerkinElmer, USA) was used to monitor the changes of fluorescence intensity of liposome-functionalized electrospun scaffolds after implantation, and the mice were anesthetized with isoflurane (2% in oxygen) during the

imaging process. For further studies on inflammatory reaction and neovascularization induced by scaffolds implantation, two targeted fluorescence imaging probes were administrated through tail vein injections. ProSense 750 FAST (PerkinElmer, USA) was activated by proteases such as Cathepsin B and was used to assess the extent of inflammatory responses. IntegriSense 645 (PerkinElmer, USA), comprising an integrin $\alpha_5\beta_3$ antagonist, was used to assess the degree of neovascularization. Exactly 4 nmol (100 μ L) of ProSense 750 FAST and 2 nmol (100 μ L) of IntegriSense 645 were administrated to a mouse and imaging was performed according to the manufacturer's instructions.

5.14. Histology and immunohistofluorescence staining

After the 14 days implantation, mice were euthanatized, and the implantation sites were isolated and fixed in 4% polyformaldehyde for the following histological analyses. After being dehydration in gradient ethanol and embedment in paraffin, all the sliced sections were subjected to hematoxylin and eosin (H&E) staining and Masson's trichrome staining to assess the cell morphology, tissue ingrowth, and collagenous fibrotic capsules formation of the scaffolds *in vivo*. For the immunohistofluorescence staining, all the sliced sections incubated with primary antibody (α -SMA, CD31, CCR7, and CD206, 1:50–1:100) at 4 °C overnight, followed by a 1 h treatment with Alexa Fluor 488/555-labeled secondary antibody. Finally, samples were rinsed with PBS and stained with 0.5 mg/mL DAPI (Sigma, USA) at room temperature for 15 min. Fluorescent images from stained scaffolds were obtained using a digital slide scanner (3DHISTECH, Hungary). Both primary antibodies and secondary antibodies for immunofluorescence were purchased from Abcam (USA). In each group, four regions were randomly selected for statistical analysis using Image-Pro Plus software.

5.15. Statistical analysis

All data were reported as the mean \pm standard deviation (SD). Statistical analysis was performed using Student's t-test and one-way analysis of variance (ANOVA), followed by the Tukey test for post hoc comparisons (OriginLab Origin 8.0 or GraphPad Prism 8 Software). *P* values less than 0.05 were considered significant.

Credit author statement

Lingbing Yang: Conceptualization, Methodology, Formal analysis, Investigation, Data curation, Writing – original draft. Xubo Lin, Methodology, Validation, Resources. Jin Zhou, Investigation, Methodology. Sen Hou, Investigation, Methodology. Yunnan Fang, Methodology. Xuwei Bi, Methodology. Li Yang, Writing – review & editing, Supervision. Linhao Li, Conceptualization, Methodology, Software, Writing – original draft, Supervision, Project administration, Funding acquisition. Yubo Fan, Writing – review & editing, Supervision, Project administration, Funding acquisition.

Declaration of competing interest

The authors declare that they have no known competing financial interests or personal relationships that could have appeared to influence the work reported in this paper.

Acknowledgments

We acknowledge the funding support from the National Natural Science Foundation of China (31971258, U20A20390, 11827803) and the 111 Project (B13003).

Appendix A. Supplementary data

Supplementary data to this article can be found online at <https://doi.org/10.1016/j.biomaterials.2021.120768>.

<https://doi.org/10.1016/j.biomaterials.2021.120768>.

Abbreviations

CHOL	cholesterol
CLSM	confocal laser scanning microscopy
DBCO	n-dibenzocyclooctyne
DLS	dynamic light scattering
DMF	n, n-dimethylformamide
DMPC	1,2-dimyristoyl-sn-glycero-3-phosphatidylcholine
DSPE	1,2-distearoyl-sn-glycero-3-phosphoethanolamine
FBGCs	foreign-body giant cells
FBR	foreign-body reaction
FDA	food and drug administration
FITC	fluorescein isothiocyanate
FRAP	fluorescence recovery after photobleaching
FTIR	Fourier transform infrared spectroscopy
H&E staining	hematoxylin and eosin staining
IFN- γ	interferon- γ
IL-4/13	interleukin-4/13
IVIS	<i>in vivo</i> imaging system
LbL	layer-by-layer
MPC	2-methacryloyloxyethyl phosphorylcholine
PC	phosphocholine
PS	polystyrene
SDS	sodium dodecyl sulfate
SEM	scanning electron microscopy
SF	silk fibroin
SPAAC	strain-promoted azide–alkyne cycloaddition
TEM	transmission electron microscopy
TLE	thin layer evaporation
TNF	tumor necrosis factor

References

- [1] B.D. Ratner, Biomaterials: been there, done that, and evolving into the future, Annu. Rev. Biomed. Eng. 21 (2019) 171–191, <https://doi.org/10.1146/annurev-bioeng-062117-120940>.
- [2] F.J. Schoen, Chapter II.2.1 - introduction: “biological responses to biomaterials, in: B.D. Ratner, A.S. Hoffman, F.J. Schoen, J.E. Lemons (Eds.), Biomater. Sci., third ed., third ed., Academic Press, 2013, pp. 499–503, <https://doi.org/10.1016/B978-0-08-087780-8.00043-7>.
- [3] S. Chen, R. Li, X. Li, J. Xie, Electrospinning: an enabling nanotechnology platform for drug delivery and regenerative medicine, Adv. Drug Deliv. Rev. 132 (2018) 188–213, <https://doi.org/10.1016/j.addr.2018.05.001>.
- [4] J. Xue, T. Wu, Y. Dai, Y. Xia, Electrospinning and electrospun nanofibers: methods, materials, and applications, Chem. Rev. 119 (2019) 5298–5415, <https://doi.org/10.1021/acs.chemrev.8b00593>.
- [5] J. Xue, D. Pisignano, Y. Xia, Maneuvering the migration and differentiation of stem cells with electrospun nanofibers, Adv. Sci. (Weinheim, Baden-Wurttemberg, Ger.) 7 (2020) 2000735, <https://doi.org/10.1002/advs.202000735>.
- [6] S. Lucke, U. Walschus, A. Hoene, M. Schnabelrauch, J.B. Nebe, B. Finke, M. Schlosser, The *in vivo* inflammatory and foreign body giant cell response against different poly(l-lactide-co-d,l-lactide) implants is primarily determined by material morphology rather than surface chemistry, J. Biomed. Mater. Res. A. 106 (2018) 2726–2734, <https://doi.org/10.1002/jbm.a.36500>.
- [7] K.M. Woo, V.J. Chen, P.X. Ma, Nano-fibrous scaffolding architecture selectively enhances protein adsorption contributing to cell attachment, J. Biomed. Mater. Res. A. 67 (2003) 531–537, <https://doi.org/10.1002/jbm.a.10098>.
- [8] J.M. Anderson, A. Rodriguez, D.T. Chang, Foreign body reaction to biomaterials, Semin. Immunol. 20 (2008) 86–100, <https://doi.org/10.1016/J.SIMI.2007.11.004>.
- [9] D. Zhang, Q. Chen, C. Shi, M. Chen, K. Ma, J. Wan, R. Liu, Dealing with the foreign-body response to implanted biomaterials: strategies and applications of new materials, Adv. Funct. Mater. 2007226 (2020) 1–22, <https://doi.org/10.1002/adfm.202007226>.
- [10] S. Al-Maawi, A. Orłowska, R. Sader, C. James Kirkpatrick, S. Ghanaati, In *vivo* cellular reactions to different biomaterials—physiological and pathological aspects and their consequences, Semin. Immunol. 29 (2017) 49–61, <https://doi.org/10.1016/j.smim.2017.06.001>.
- [11] K. Garg, N.A. Pullen, C.A. Oskeritzian, J.J. Ryan, G.L. Bowlin, Macrophage functional polarization (M1/M2) in response to varying fiber and pore dimensions of electrospun scaffolds, Biomaterials 34 (2013) 4439–4451, <https://doi.org/10.1016/j.biomaterials.2013.02.065>.

- [12] E.M. Sussman, M.C. Halpin, J. Muster, R.T. Moon, B.D. Ratner, Porous implants modulate healing and induce shifts in local macrophage polarization in the foreign body reaction, *Ann. Biomed. Eng.* 42 (2014) 1508–1516, <https://doi.org/10.1007/s10439-013-0933-0>.
- [13] R. Sridharan, B. Cavanagh, A.R. Cameron, D.J. Kelly, F.J. O'Brien, Material stiffness influences the polarization state, function and migration mode of macrophages, *Acta Biomater.* 89 (2019) 47–59, <https://doi.org/10.1016/j.actbio.2019.02.048>.
- [14] K. Sadtler, M.T. Wolf, S. Ganguly, C.A. Moad, L. Chung, S. Majumdar, F. Housseau, D.M. Pardoll, J.H. Elisseeff, Divergent immune responses to synthetic and biological scaffolds, *Biomaterials* 192 (2019) 405–415, <https://doi.org/10.1016/j.biomaterials.2018.11.002>.
- [15] O. Veiseh, J.C. Doloff, M. Ma, A.J. Vegas, H.H. Tam, A.R. Bader, J. Li, E. Langan, J. Wyckoff, W.S. Loo, S. Jhunjhunwala, A. Chiu, S. Siebert, K. Tang, J. Hollister-Lock, S. Aresta-Dasilva, M. Bochenek, J. Mendoza-Elias, Y. Wang, M. Qi, D. M. Lavin, M. Chen, N. Dholakia, R. Thakrar, I. Lacik, G.C. Weir, J. Oberholzer, D. L. Greiner, R. Langer, D.G. Anderson, Size- and shape-dependent foreign body immune response to materials implanted in rodents and non-human primates, *Nat. Mater.* 14 (2015) 643–651, <https://doi.org/10.1038/nmat4290>.
- [16] F.Y. McWhorter, T. Wang, P. Nguyen, T. Chung, W.F. Liu, Modulation of macrophage phenotype by cell shape, *Proc. Natl. Acad. Sci. U. S. A* 110 (2013) 17253–17258, <https://doi.org/10.1073/pnas.1308887110>.
- [17] M.J. Vassey, G.P. Figueiredo, D.J. Scurr, A.S. Vasilevich, S. Vermeulen, A. Carlier, J. Luckett, N.R.M. Beijer, P. Williams, D.A. Winkler, J. de Boer, A. M. Ghaemmaghami, M.R. Alexander, Immune modulation by design: using topography to control human monocyte attachment and macrophage differentiation, *Adv. Sci. (Weinheim, Baden-Württemberg, Ger.)* 7 (2020) 1903392, <https://doi.org/10.1002/advs.201903392>.
- [18] N. Jain, V. Vogel, Spatial confinement downsizes the inflammatory response of macrophages, *Nat. Mater.* 17 (2018) 1134–1144, <https://doi.org/10.1038/s41563-018-0190-6>.
- [19] A.J. Vegas, O. Veiseh, J.C. Doloff, M. Ma, H.H. Tam, K. Bratlie, J. Li, A.R. Bader, E. Langan, K. Olejnik, P. Fenton, J.W. Kang, J. Hollister-Locke, M.A. Bochenek, A. Chiu, S. Siebert, K. Tang, S. Jhunjhunwala, S. Aresta-Dasilva, N. Dholakia, R. Thakrar, T. Vietti, M. Chen, J. Cohen, K. Siniakowicz, M. Qi, J. McGarrigle, A. C. Graham, S. Lyle, D.M. Harlan, D.L. Greiner, J. Oberholzer, G.C. Weir, R. Langer, D.G. Anderson, Combinatorial hydrogel library enables identification of materials that mitigate the foreign body response in primates, *Nat. Biotechnol.* 34 (2016) 345–352, <https://doi.org/10.1038/nbt.3462>.
- [20] M. Ma, W.F. Liu, P.S. Hill, K.M. Bratlie, D.J. Siegwart, J. Chin, M. Park, J. Guerreiro, D.G. Anderson, Development of cationic polymer coatings to regulate foreign-body responses, *Adv. Mater.* 23 (2011) H189–H194, <https://doi.org/10.1002/adma.201100513>.
- [21] Q. Liu, A. Chiu, L. Wang, D. An, W. Li, E.Y. Chen, Y. Zhang, Y. Pardo, S. P. McDonough, L. Liu, W.F. Liu, J. Chen, M. Ma, Developing mechanically robust, triazole-zwitterionic hydrogels to mitigate foreign body response (FBR) for islet encapsulation, *Biomaterials* 230 (2020) 119640, <https://doi.org/10.1016/j.biomaterials.2019.119640>.
- [22] L. Zhang, Z. Cao, T. Bai, L. Carr, J.-R. Ella-Menyé, C. Irvin, B.D. Ratner, S. Jiang, Zwitterionic hydrogels implanted in mice resist the foreign-body reaction, *Nat. Biotechnol.* 31 (2013) 553–556, <https://doi.org/10.1038/nbt.2580>.
- [23] H. Yan, C. Seignez, M. Hjorth, B. Winkeljann, M. Blakeley, O. Lieleg, M. Phillipson, T. Crouzier, Immune-informed mucin hydrogels evade fibrotic foreign body response in vivo, *Adv. Funct. Mater.* 29 (2019) 1–11, <https://doi.org/10.1002/adfm.201902581>.
- [24] Y.J. Du, J.L. Brash, G. McClung, L.R. Berry, P. Klement, A.K.C. Chan, Protein adsorption on polyurethane catheters modified with a novel antithrombin-heparin covalent complex, *J. Biomed. Mater. Res.* 80A (2007) 216–225, <https://doi.org/10.1002/jbm.a.30977>.
- [25] S.J. Geelhood, T.A. Horbett, W.K. Ward, M.D. Wood, M.J. Quinn, Passivating protein coatings for implantable glucose sensors: evaluation of protein retention, *J. Biomed. Mater. Res. B Appl. Biomater.* 81B (2007) 251–260, <https://doi.org/10.1002/jbm.b.30660>.
- [26] R.M. Gower, R.M. Boehler, S.M. Azarin, C.F. Ricci, J.N. Leonard, L.D. Shea, Modulation of leukocyte infiltration and phenotype in microporous tissue engineering scaffolds via vector induced IL-10 expression, *Biomaterials* 35 (2014) 2024–2031, <https://doi.org/10.1016/j.biomaterials.2013.11.036>.
- [27] K.L. Spiller, S. Nassiri, C.E. Witherel, R.R. Anfang, J. Ng, K.R. Nakazawa, T. Yu, G. Vunjak-Novakovic, Sequential delivery of immunomodulatory cytokines to facilitate the M1-to-M2 transition of macrophages and enhance vascularization of bone scaffolds, *Biomaterials* 37 (2015) 194–207, <https://doi.org/10.1016/j.biomaterials.2014.10.017>.
- [28] S. Minardi, B. Corradetti, F. Taraballini, J.H. Byun, F. Cabrera, X. Liu, M. Ferrari, B. K. Weiner, E. Tasciotti, IL-4 release from a biomimetic scaffold for the temporally controlled modulation of macrophage response, *Ann. Biomed. Eng.* 44 (2016) 2008–2019, <https://doi.org/10.1007/s10439-016-1580-z>.
- [29] J. Weingart, P. Vabbilisetty, X.-L. Sun, Membrane mimetic surface functionalization of nanoparticles: methods and applications, *Adv. Colloid Interface Sci.* 197–198 (2013) 68–84, <https://doi.org/10.1016/j.cis.2013.04.003>.
- [30] R.H. Fang, A. V Kroll, W. Gao, L. Zhang, Cell membrane coating nanotechnology, *Adv. Mater.* 30 (2018), e1706759, <https://doi.org/10.1002/adma.201706759>.
- [31] R.H. Fang, Y. Jiang, J.C. Fang, L. Zhang, Cell membrane-derived nanomaterials for biomedical applications, *Biomaterials* 128 (2017) 69–83, <https://doi.org/10.1016/j.biomaterials.2017.02.041>.
- [32] R. Cheng, L. Liu, Y. Xiang, Y. Lu, L. Deng, H. Zhang, H.A. Santos, W. Cui, Advanced liposome-loaded scaffolds for therapeutic and tissue engineering applications, *Biomaterials* 232 (2020), 119706, <https://doi.org/10.1016/j.biomaterials.2019.119706>.
- [33] T.M. Allen, P.R. Cullis, Liposomal drug delivery systems: from concept to clinical applications, *Adv. Drug Deliv. Rev.* 65 (2013) 36–48, <https://doi.org/10.1016/j.addr.2012.09.037>.
- [34] N. Filipczak, J. Pan, S.S.K. Yalamarty, V.P. Torchilin, Recent advancements in liposome technology, *Adv. Drug Deliv. Rev.* (2020) 1–19, <https://doi.org/10.1016/j.addr.2020.06.022>.
- [35] J.A. Jackman, N.J. Cho, Supported lipid bilayer formation: beyond vesicle fusion, *Langmuir* 36 (2020) 1387–1400, <https://doi.org/10.1021/acs.langmuir.9b03706>.
- [36] Z. Zha, C. Cohn, Z. Dai, W. Qiu, J. Zhang, X. Wu, Nanofibrous lipid membranes capable of functionally immobilizing antibodies and capturing specific cells, *Adv. Mater.* 23 (2011) 3435–3440, <https://doi.org/10.1002/adma.201101516>.
- [37] K. Fotiadis, E. Filidou, K. Arvanitidis, V. Valatas, G. Stavrou, G. Basdanis, V. Paspaliaris, G. Kolios, K. Kotzampassi, Intraperitoneal application of phospholipids for the prevention of postoperative adhesions: a possible role of myofibroblasts, *J. Surg. Res.* 197 (2015) 291–300, <https://doi.org/10.1016/j.jss.2015.04.036>.
- [38] M.K. Sabnani, R. Rajan, B. Rowland, V. Mavinkurve, L.M. Wood, A.A. Gabizon, N. M. La-Beck, Liposome promotion of tumor growth is associated with angiogenesis and inhibition of antitumor immune responses, *Nanomed. Nanotechnol. Biol. Med.* 11 (2015) 259–262, <https://doi.org/10.1016/j.nano.2014.08.010>.
- [39] R. Rajan, M.K. Sabnani, V. Mavinkurve, H. Shmeeda, H. Mansouri, S. Bonkoungou, A.D. Le, L.M. Wood, A.A. Gabizon, N.M. La-Beck, Liposome-induced immunosuppression and tumor growth is mediated by macrophages and mitigated by liposome-encapsulated alendronate, *J. Contr. Release* 271 (2018) 139–148, <https://doi.org/10.1016/j.jconrel.2017.12.023>.
- [40] L. Li, S. Puhl, L. Meinel, O. Germershaus, Silk fibroin layer-by-layer microcapsules for localized gene delivery, *Biomaterials* 35 (2014) 7929–7939, <https://doi.org/10.1016/j.biomaterials.2014.05.062>.
- [41] Y. Qian, L. Li, Y. Song, L. Dong, P. Chen, X. Li, K. Cai, O. Germershaus, L. Yang, Y. Fan, Surface modification of nanofibrous matrices via layer-by-layer functionalized silk assembly for mitigating the foreign body reaction, *Biomaterials* 164 (2018) 22–37, <https://doi.org/10.1016/j.biomaterials.2018.02.038>.
- [42] A.S. Cheung, D.K.Y. Zhang, S.T. Koshy, D.J. Mooney, Scaffolds that mimic antigen-presenting cells enable ex vivo expansion of primary T cells, *Nat. Biotechnol.* 36 (2018) 160–169, <https://doi.org/10.1038/nbt.4047>.
- [43] B.R. Olden, C.R. Perez, A.L. Wilson, I.I. Cardle, Y.S. Lin, B. Kaepr, J.A. Gustafson, M.C. Jensen, S.H. Pun, Cell-templated silica microparticles with supported lipid bilayers as artificial antigen-presenting cells for T cell activation, *Adv. Healthc. Mater.* 8 (2019) 1–8, <https://doi.org/10.1002/adhm.201801188>.
- [44] J.S. Duffield, M. Luper, V.J. Thannickal, T.A. Wynn, Host responses in tissue repair and fibrosis, *Annu. Rev. Pathol.* 8 (2013) 241–276, <https://doi.org/10.1146/annurev-pathol-020712-163930>.
- [45] T.A. Wynn, K.M. Vannella, Macrophages in tissue repair, regeneration, and fibrosis, *Immunity* 44 (2016) 450–462, <https://doi.org/10.1016/j.immuni.2016.02.015>.
- [46] X. Fu, Y. Lu, J. Guo, H. Liu, A. Deng, C. Kuang, X. Xie, K237-modified thermosensitive liposome enhanced the delivery efficiency and cytotoxicity of paclitaxel in vitro, *J. Liposome Res.* 29 (2019) 86–93, <https://doi.org/10.1080/089282104.2018.1458863>.
- [47] I. Takeuchi, Y. Kanno, H. Uchiyo, K. Makino, Polyborane-encapsulated PEGylated liposomes prepared using post-insertion technique for boron neutron capture therapy, *J. Oleo Sci.* 68 (2019) 1261–1270, <https://doi.org/10.5650/josess.19218>.
- [48] Y.-Z. Zhao, D.-L. ZhuGe, M.-Q. Tong, M.-T. Lin, Y.-W. Zheng, X. Jiang, W.-G. Yang, Q. Yao, Q. Xiang, X.-K. Li, H.-X. Xu, Ulcerative colitis-specific delivery of keratinocyte growth factor by neutrophils-simulated liposomes facilitates the morphologic and functional recovery of the damaged colon through alleviating the inflammation, *J. Contr. Release* 299 (2019) 90–106, <https://doi.org/10.1016/j.jconrel.2019.02.034>.
- [49] Y. Zhao, A. Liu, Y. Du, Y. Cao, E. Zhang, Q. Zhou, H. Hai, Y. Zhen, S. Zhang, Effects of sucrose ester structures on liposome-mediated gene delivery, *Acta Biomater.* 72 (2018) 278–286, <https://doi.org/10.1016/j.actbio.2018.03.031>.
- [50] N. Monteiro, M. Martins, A. Martins, N.A. Fonseca, J.N. Moreira, R.L. Reis, N. M. Neves, Antibacterial activity of chitosan nanofiber meshes with liposomes immobilized releasing gentamicin, *Acta Biomater.* 18 (2015) 196–205, <https://doi.org/10.1016/j.actbio.2015.02.018>.
- [51] R. Chandrawati, M.T.J. Olesen, T.C.C. Marini, G. Bisra, A.G. Guex, M.G. de Oliveira, A.N. Zelikin, M.M. Stevens, Enzyme prodrug therapy engineered into electrospun fibers with embedded liposomes for controlled, localized synthesis of therapeutics, *Adv. Healthc. Mater.* 6 (2017), <https://doi.org/10.1002/adhm.201700385>.
- [52] K. Xi, Y. Gu, J. Tang, H. Chen, Y. Xu, L. Wu, F. Cai, L. Deng, H. Yang, Q. Shi, W. Cui, L. Chen, Microenvironment-responsive immunoregulatory electrospun fibers for promoting nerve function recovery, *Nat. Commun.* 11 (2020) 4504, <https://doi.org/10.1038/s41467-020-18265-3>.
- [53] L. Duque Sánchez, N. Brack, A. Postma, P.J. Pigram, L. Meagher, Surface modification of electrospun fibres for biomedical applications: a focus on radical polymerization methods, *Biomaterials* 106 (2016) 24–45, <https://doi.org/10.1016/j.biomaterials.2016.08.011>.
- [54] L. Pasquardini, L. Lunelli, L. Vanzetti, M. Anderle, C. Pederzoli, Immobilization of cationic rifampicin-loaded liposomes on polystyrene for drug-delivery applications, *Colloids Surf. B Biointerfaces* 62 (2008) 265–272, <https://doi.org/10.1016/j.colsurfb.2007.10.019>.
- [55] K. Ishihara, N.P. Ziats, B.P. Tierney, N. Nakabayashi, J.M. Anderson, Protein adsorption from human plasma is reduced on phospholipid polymers, *J. Biomed. Mater. Res.* 25 (1991) 1397–1407, <https://doi.org/10.1002/jbm.820251107>.

- [56] K. Ishihara, H. Nomura, T. Mihara, K. Kurita, Y. Iwasaki, N. Nakabayashi, Why do phospholipid polymers reduce protein adsorption? *J. Biomed. Mater. Res.* 39 (1998) 323–330, [https://doi.org/10.1002/\(sici\)1097-4636_19980239;2<323::aid-jbm21>3.0.co;2-c](https://doi.org/10.1002/(sici)1097-4636_19980239;2<323::aid-jbm21>3.0.co;2-c).
- [57] S. Kang, J. Kim, S. Kim, M. Wufuer, S. Park, Y. Kim, D. Choi, X. Jin, Y. Kim, Y. Huang, B. Jeon, T.H. Choi, J.-U. Park, Y. Lee, Efficient reduction of fibrous capsule formation around silicone breast implants densely grafted with 2-methacryloyloxyethyl phosphorylcholine (MPC) polymers by heat-induced polymerization, *Biomater. Sci.* 8 (2020) 1580–1591, <https://doi.org/10.1039/c9bm01802f>.
- [58] K. Ishihara, Revolutionary advances in 2-methacryloyloxyethyl phosphorylcholine polymers as biomaterials, *J. Biomed. Mater. Res. A* 107 (2019) 933–943, <https://doi.org/10.1002/jbm.a.36635>.
- [59] K. Ishihara, Blood-compatible surfaces with phosphorylcholine-based polymers for cardiovascular medical devices, *Langmuir* 35 (2019) 1778–1787, <https://doi.org/10.1021/acs.langmuir.8b01565>.
- [60] R. Toita, E. Shimizu, M. Murata, J.-H. Kang, Protective and healing effects of apoptotic mimic-induced M2-like macrophage polarization on pressure ulcers in young and middle-aged mice, *J. Contr. Release* 330 (2021) 705–714, <https://doi.org/10.1016/j.jconrel.2020.12.052>.
- [61] N. Xu, J. Li, Y. Gao, N. Zhou, Q. Ma, M. Wu, Y. Zhang, X. Sun, J. Xie, G. Shen, M. Yang, Q. Tu, X. Xu, J. Zhu, J. Tao, Apoptotic cell-mimicking gold nanocages loaded with LXR agonist for attenuating the progression of murine systemic lupus erythematosus, *Biomaterials* 197 (2019) 380–392, <https://doi.org/10.1016/j.biomaterials.2019.01.034>.
- [62] J.E. Tengood, K.M. Kovach, P.E. Vescovi, A.J. Russell, S.R. Little, Sequential delivery of vascular endothelial growth factor and sphingosine 1-phosphate for angiogenesis, *Biomaterials* 31 (2010) 7805–7812, <https://doi.org/10.1016/j.biomaterials.2010.07.010>.
- [63] L.S. Sefcik, C.E. Petrie Aronin, K.A. Wieghaus, E.A. Botchwey, Sustained release of sphingosine 1-phosphate for therapeutic arteriogenesis and bone tissue engineering, *Biomaterials* 29 (2008) 2869–2877, <https://doi.org/10.1016/j.biomaterials.2008.03.017>.
- [64] P.J. Murray, Macrophage polarization, *Annu. Rev. Physiol.* 79 (2017) 541–566, <https://doi.org/10.1146/annurev-physiol-022516-034339>.
- [65] L. Davenport Huyer, S. Pascual-Gil, Y. Wang, S. Mandla, B. Yee, M. Radisic, Advanced strategies for modulation of the material–macrophage interface, *Adv. Funct. Mater.* 30 (2020) 1–21, <https://doi.org/10.1002/adfm.201909331>.
- [66] N.M. La-Beck, A.A. Gabizon, Nanoparticle interactions with the immune system: clinical implications for liposome-based cancer chemotherapy, *Front. Immunol.* 8 (2017) 416, <https://doi.org/10.3389/fimmu.2017.00416>.
- [67] H. Zhao, E. Heusler, G. Jones, L. Li, V. Werner, O. Germershaus, J. Ritzer, T. Luehmann, L. Meinel, Decoration of silk fibroin by click chemistry for biomedical application, *J. Struct. Biol.* 186 (2014), <https://doi.org/10.1016/j.jsb.2014.02.009>.
- [68] S.J. Marrink, H.J. Risselada, S. Yefimov, D.P. Tieleman, A.H. de Vries, The MARTINI force field: coarse grained model for biomolecular simulations, *J. Phys. Chem. B* 111 (2007) 7812–7824, <https://doi.org/10.1021/jp071097f>.
- [69] D.H. de Jong, G. Singh, W.F.D. Bennett, C. Arnarez, T.A. Wassenaar, L. V Schäfer, X. Periole, D.P. Tieleman, S.J. Marrink, Improved parameters for the Martini coarse-grained protein force field, *J. Chem. Theor. Comput.* 9 (2013) 687–697, <https://doi.org/10.1021/ct300646g>.
- [70] M. Patel, D.K. Dubey, S.P. Singh, Phenomenological models of Bombyx mori silk fibroin and their mechanical behavior using molecular dynamics simulations, *Mater. Sci. Eng. C. Mater. Biol. Appl.* 108 (2020) 110414, <https://doi.org/10.1016/j.msec.2019.110414>.
- [71] J. Lee, X. Cheng, J.M. Swails, M.S. Yeom, P.K. Eastman, J.A. Lemkul, S. Wei, J. Buckner, J.C. Jeong, Y. Qi, S. Jo, V.S. Pande, D.A. Case, C.L. 3rd Brooks, A.D. J. MacKerell, J.B. Klauda, W. Im, CHARMM-GUI input generator for NAMD, GROMACS, AMBER, OpenMM, and CHARMM/OpenMM simulations using the CHARMM36 additive force field, *J. Chem. Theor. Comput.* 12 (2016) 405–413, <https://doi.org/10.1021/acs.jctc.5b00935>.